DR. 71

ORNL/TM-6992

A Theoretical Study of Electron-Cyclotron Heating in Elmo Bumpy Torus

D. B. Batchelor
R. C. Goldfinger

OAK RIDGE NATIONAL LABORATORY
OPERATED BY UNION CARBIDE CORPORATION · FOR THE DEPARTMENT OF ENERGY

ORNL/TM-6992
Dist. Category UC-20 g

Contract No. W-7405-eng-26

A THEORETICAL STUDY OF ELECTRON-CYCLOTRON HEATING IN ELMO BUMPY TORUS

D. B. Batchelor
Fusion Energy Division

and

R. C. Goldfinger
Computer Sciences Division

Date Published - September 1979

Prepared by the
OAK RIDGE NATIONAL LABORATORY
Oak Ridge, Tennessee 37830
operated by
UNION CARBIDE CORPORATION
for the
DEPARTMENT OF ENERGY

CONTENTS

ABSTRACT

The basic features of microwave propagation and electron-cyclotron damping in ELMO Bumpy Torus (EBT) devices are investigated to provide an understanding of the heating of the toroidal core plasma component. The characteristics of microwave propagation in EBT geometry, where there is strong variation of $|\underset{\sim}{B}|$ along field lines, are described and contrast is made with the electron-cyclotron heating (ECH) of tokamaks. Linear cyclotron damping calculations are presented for plasmas having parameters typical of EBT-I and parameters projected for EBT-II. It is shown that the extraordinary mode is completely absorbed near the fundamental cyclotron resonance when propagating from the high magnetic field side (mirror throat). For EBT-I parameters, heating by the ordinary mode at the fundamental cyclotron resonance and by both modes at the second harmonic resonance is negligible. For projected EBT-II parameters, the ordinary mode is heavily damped at the fundamental and the extraordinary mode is heavily damped at the second harmonic. Since the right-hand cutoff prevents injected extraordinary mode energy from propagating to the cyclotron resonance, a mechanism must exist outside of geometrical optics by which the extraordinary mode reaches resonance. It is argued that this mechanism is the conversion of ordinary mode energy to extraordinary mode in the high field region upon wall reflection.

1. INTRODUCTION

In the ELMO Bumpy Torus (EBT) device [1,2], all heating is provided by microwaves through the electron-cyclotron resonance interaction. In addition, the microwaves play an essential role by producing the high beta, hot electron annuli which provide macroscopic stability for the toroidal plasma component. A knowledge of the microwave field distribution and heating profile is crucial to the understanding of EBT physics.

EBT-I consists of 24 toroidally linked mirror sectors having a 2:1 mirror ratio and a peak field strength on axis at the mirror throat of 13 kG. The magnetic geometry is illustrated in Fig. 1, which shows the vacuum field lines (solid) and contours of constant $|\underset{\sim}{B}|$ in the equatorial plane for a sector of EBT. Steady-state plasma is formed and heated by an ECH microwave source providing up to 60 kW at a frequency of 18 GHz and a lower, off-resonance heating source providing up to 30 kW at 10.6 GHz. The current in the mirror coils is adjusted so as to produce cyclotron resonance zones $\omega = \Omega_e(\underset{\sim}{x}) = e|\underset{\sim}{B}(x)|/m_e c$ as indicated in Fig. 1. High beta annuli consisting of relativistic electrons ($T_{eAnnulus} \sim$ 200 keV) form at the midplane of each mirror sector in the vicinity of the second harmonic resonance for the 18-GHz microwaves. In addition to the high beta annuli, the EBT plasma contains a toroidal core component of much higher density ($n_{eCore} \gtrsim 10\ n_{eAnnulus}$) and lower temperature ($T_{eCore} \sim$ 150-600 eV) confined by the bumpy torus magnetic field configuration [3]. There is now great interest in the transport and scaling properties of the toroidal core plasma in EBT to assess its potential as a fusion reactor [4,5]. In this paper, therefore, we will concentrate on the cyclotron damping of the 18-GHz microwaves by the higher density

BLANK PAGE

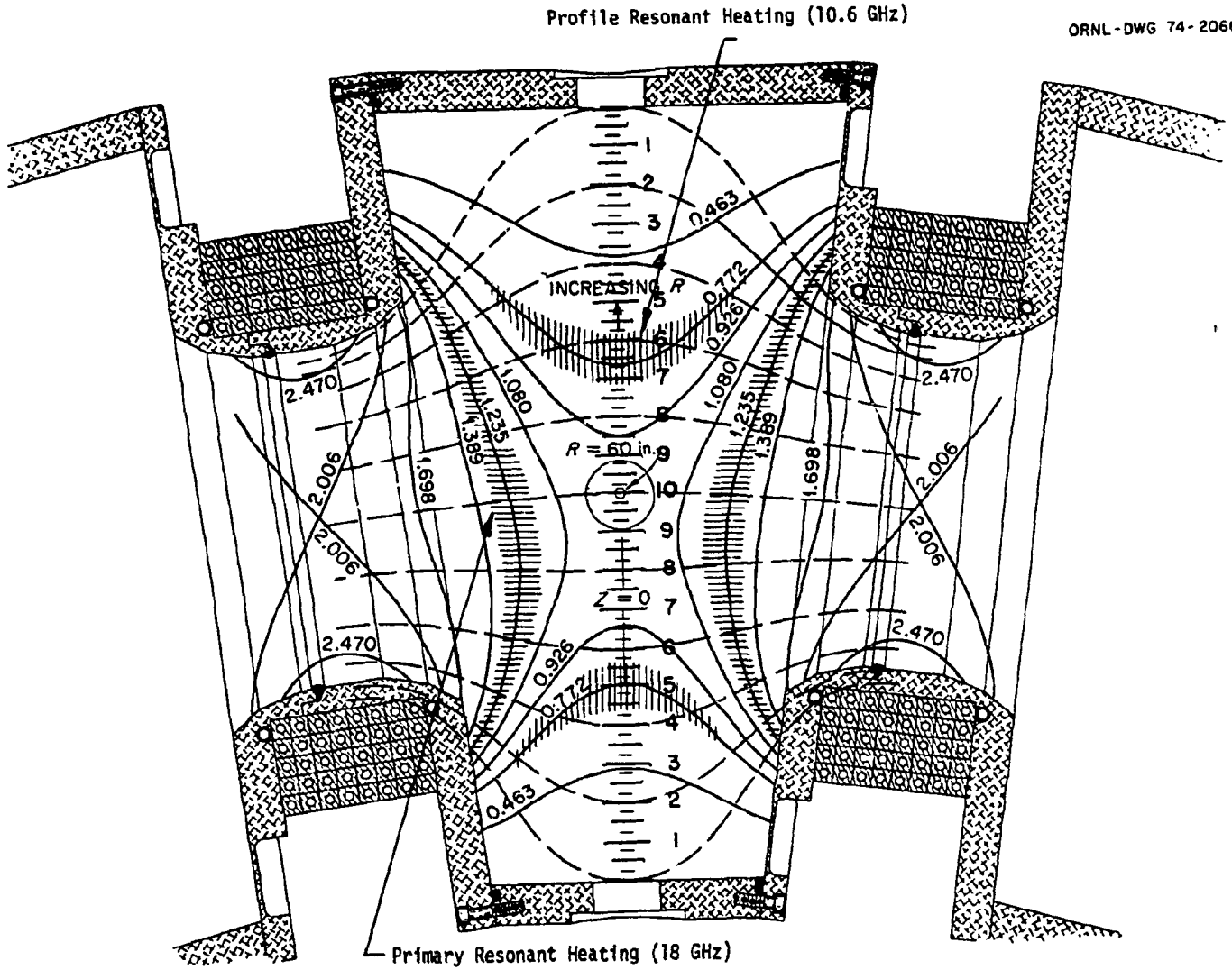

EBT Mod-B Contours (—), Flux Lines (---), and Heating Geometry (//////)

Fig. 1

toroidal core plasma. Relativistic calculations of absorption by the hot electron annuli are currently under way and will be reported separately.

A number of previous studies have dealt with the theory of electron-cyclotron heating in axisymmetric mirror machines [6-10] where the heating was calculated from single particle orbits or from a Fokker-Planck-type equation. The microwave field was assumed to be a cavity normal mode or some arbitrarily specified field structure, and the plasma density was assumed to be sufficiently low that plasma currents produce only small perturbations in the wave fields. However, the volume of the EBT vacuum vessel is so large ($V = 1.3\ m^3 \sim 10^5\ \lambda^3$, where λ = microwave free space wavelength) that cavity modes cannot be expected to play any role, and the unperturbed field structure is certainly not known. In addition, the plasma density is sufficiently high ($\omega_{pe}^2 c/\Omega_e^2 v_e \gg 1$) that plasma currents strongly affect wave propagation throughout the machine. Indeed, in EBT plasma resonances and cutoffs dominate the propagation characteristics of the microwave power.

Other studies have investigated electron-cyclotron heating in tokamak geometry [11-16]. Usually these studies have made simplifying assumptions on the geometry, such as plane stratification. In EBT, however, the plasma and cavity have a very complicated and unsymmetrical structure (refer to Fig. 1); thus, the assumption of plane stratification is inadequate, and more detailed calculations are necessary in order to determine the spatial heating profiles. A large scale computational effect is now in progress to trace the microwave energy flow and heating characteristics of EBT using geometrical optics [17]; some preliminary results of this work are reported here.

In Section 2 of this report, we discuss the wave propagation properties of the ordinary and extraordinary modes in EBT geometry. A dominant feature is the presence of the right-hand cutoff, which prevents the extraordinary mode from propagating directly to the cyclotron resonance layer from the mirror midplane, where the waves are injected. This unavoidable cutoff and the presence of strong gradients in magnetic field strength along the field lines make the electron-cyclotron heating of EBT entirely different from that of tokamaks. We consider in some detail two cases of plane-stratified plasma: (1) perpendicular stratified plasma (gradients perpendicular to $\underset{\sim}{B}$, characteristic of tokamaks) and (2) parallel stratified plasma (gradients purely along $\underset{\sim}{B}$, characteristic of fundamental resonance in EBT). For extraordinary mode propagation in a parallel stratified plasma, the wave vector $\underset{\sim}{k}$ turns parallel to $\underset{\sim}{B}$ as the wave approaches cyclotron resonance. This results in enormous absorption in a dense plasma.

The energy deposition is evaluated by integrating the imaginary part of the refractive index k_i along geometrical optics ray paths. In Section 3, we discuss the finite temperature dispersion relation used and indicate some of the complications which arise when the gradients in plasma parameters are not perpendicular to $\underset{\sim}{B}$ or when the plasma is not plane stratified. It is shown that when the waves are not too heavily damped, the absorption predicted by integrating $\underset{\sim}{k}_i$ along the ray is independent of the direction chosen for $\underset{\sim}{k}_i$.

Calculations are presented in Section 4 showing damping rates and fractional power absorption at the cyclotron and second harmonic resonances in plane-stratified plasmas typical of EBT-I and projected

parameters for EBT-II. We find that absorption of the ordinary mode by the core plasma of EBT-I is negligible throughout. On the other hand, the extraordinary mode is strongly damped at the cyclotron resonance but weakly damped at the second harmonic. For plasma parameters expected in EBT-II, the situation is entirely different. The ordinary mode is heavily damped in the hot, dense core region. Also, the extraordinary mode is significantly damped by the core plasma in the region of the second harmonic resonance. These results for plane-stratified geometry are borne out by calculations in a more realistic magnetic mirror geometry. In Section 5, we discuss fractional absorption calculations made with a geometrical optics code using a bumpy cylinder equilibrium model.

In Section 6 we summarize the results and construct a qualitative picture of the electron-cyclotron heating of the core plasma in EBT. Because the extraordinary mode energy injected near the mirror midplane is cut off before reaching the cyclotron resonance and the ordinary mode does not significantly heat the core plasma in EBT-I, some mechanism must exist outside the geometrical optics model whereby extraordinary mode energy is transmitted to the high field region. The most likely candidate appears to be the conversion of ordinary mode to extraordinary mode in the high field region.

2. ENERGY TRANSPORT CONSIDERATIONS

The transport of energy throughout the EBT plasma, as distinguished from the actual deposition of energy, can adequately be understood using cold plasma wave theory. The cold plasma dispersion relation in the electron-cyclotron frequency regime $\omega \sim \Omega_e \gg \Omega_i, \omega_{pi}$ is conveniently expressed in the Appleton-Hartree form [18]

$$n^2 = 1 - \frac{2\alpha(1 - \alpha)}{2(1 - \alpha) - \beta \sin^2 \theta \pm \Gamma} \tag{1}$$

where

$n = ck/\omega$ = wave refractive index

$$\alpha = \frac{\omega_{pe}^2}{\omega} = \frac{4\pi n_e e^2}{m_e \omega^2}, \qquad \beta = \frac{\Omega_e^2}{\omega^2}$$

$$\Gamma = [\beta^2 \sin^4 \theta + 4\beta(1 - \alpha)^2 \cos^2 \theta]^{1/2}$$

$$\theta = \cos^{-1}(\underset{\sim}{k} \cdot \underset{\sim}{B}/|\underset{\sim}{k}|\ |\underset{\sim}{B}|)$$

and the +(-) signs refer to ordinary (extraordinary) mode propagation. A resonance, $n \to \infty$, occurs in the extraordinary mode branch at a magnetic field strength β_R which depends on the density and angle of propagation, $\beta_R = (1 - \alpha)(1 - \alpha \cos^2 \theta)^{-1}$. The extraordinary mode cutoff or right-hand cutoff, $n \to 0$, occurs at the magnetic field strength $\beta_C = (1 - \alpha)^2$, for which the extraordinary mode does not propagate at any angle θ. Thus an extraordinary mode wave propagating toward the cyclotron resonance from a low magnetic field region ($\beta < \beta_C < \beta_R$) will be reflected at or before it reaches the right-hand cutoff layer.

Since EBT operates in a density regime such that $\alpha < 1$, there are no resonances or cutoffs for the ordinary mode. In fact, ray tracing studies show that ordinary mode waves are barely refracted in EBT plasmas. It is anticipated that future devices will also operate in this $\alpha < 1$ regime.

Figure 2 shows a cross section of an EBT sector with a high beta (β = 40%) annulus plasma calculated using a 3-D tensor-pressure equilibrium code. An ad hoc model was adopted for the low beta core plasma density profile. In this model, the density is constant along magnetic field lines, is maximum on axis, decreases slowly with radius out to the high beta annulus, and then drops sharply to a constant value outside the annulus. The peak electron density is known experimentally to be $1\text{-}2 \times 10^{12}$ cm^{-3}, whereas the density near the surface is $n_e \sim 2 \times 10^{11}$ cm^{-3}. Shown in Fig. 2 are magnetic field lines, 18-GHz first and second harmonic cyclotron resonant zones, and the right-hand cutoff. The resonance and cutoff surfaces are distorted by the presence of the magnetic well. It is clear that extraordinary mode energy, propagating from the midplane region (where the microwaves are injected), is reflected from the right-hand cutoff before reaching the fundamental cyclotron resonant surface.

For the case shown in Fig. 2, the peak density was chosen to be $n_e = 2 \times 10^{12}$ cm^{-3} [i.e., $\alpha(r = 0) = 1/2$]. For this or lower density, the second harmonic resonance is accessible to the extraordinary mode. In a sequence of experiments with electron-cyclotron heated mirror plasmas having high beta rings, a maximum density limit was observed at about half the ordinary mode cutoff density. We conjecture that this is

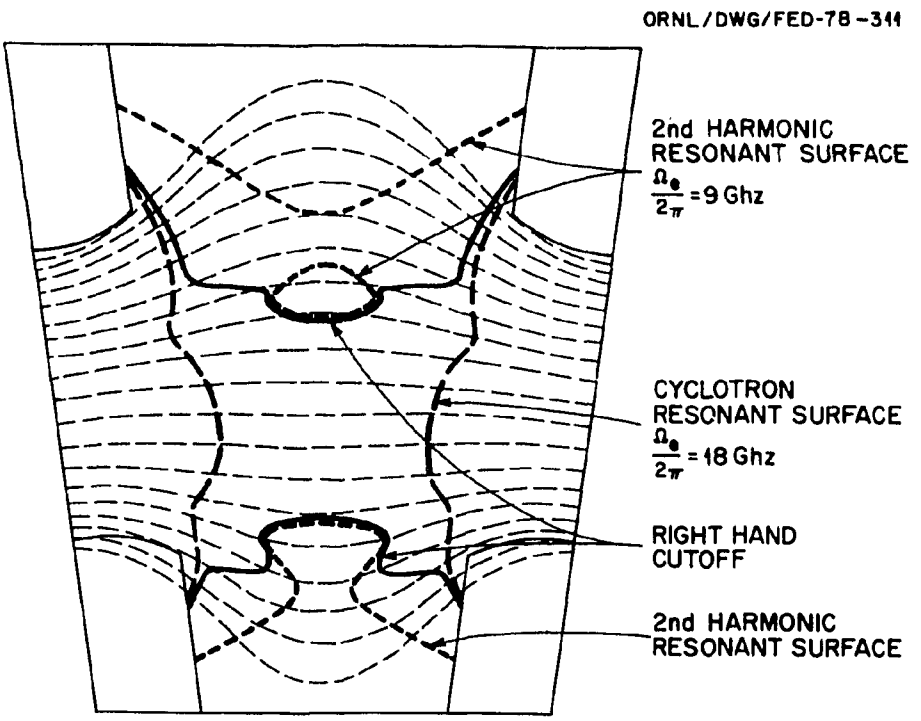
ORNL/DWG/FED-78-344
2nd HARMONIC
RESONANT SURFACE
$\frac{\Omega_e}{2\pi}$ = 9 Ghz
CYCLOTRON
RESONANT SURFACE
$\frac{\Omega_e}{2\pi}$ = 18 Ghz
RIGHT HAND
CUTOFF
2nd HARMONIC
RESONANT SURFACE

Fig. 2

related to the condition for extraordinary mode accessibility to the second harmonic resonance, i.e., $\alpha < 1/2$. At higher density, extraordinary mode heating of the annulus would be reduced and annulus beta could not be maintained.

Although the fundamental cyclotron resonance is inaccessible to the injected extraordinary mode waves, it is observed experimentally that significant heating of the core plasma does, in fact, occur. The cyclotron resonant surface is accessible to the ordinary mode, but, as shown later, the ordinary mode is not absorbed. Therefore, a mechanism must exist for extraordinary mode energy to propagate to the resonant surface. In Section 6, it is argued that this mechanism is the conversion of ordinary mode energy to extraordinary mode in the high field region by means of wall reflections.

The amount of cyclotron damping which a wave experiences in passing through cyclotron resonance is strongly dependent on θ, the angle between $\underset{\sim}{k}$ and $\underset{\sim}{B}$ at the resonance layer. This angle is not actually under the experimenters' control, but is sensitively dependent on the plasma geometry as well as on the $\underset{\sim}{k}$ spectrum of injected waves. For complicated plasma geometry it is necessary to use the methods of ray tracing to determine the direction of $\underset{\sim}{k}$ throughout the plasma. Considerable simplification is obtained if one assumes that the plasma has a plane-stratified geometry (i.e., all gradients are in a fixed direction). In that case, the refractive index in any direction perpendicular to the gradients is constant as a consequence of Snell's law. We will consider two examples of plane-stratified plasmas which serve to illustrate some of the important differences between wave propagation and absorption in tokamaks vs EBT.

For many purposes the plasma in a tokamak is adequately modeled as a slab with straight magnetic field lines $\underset{\sim}{B}$ along the z direction and all gradients of $|B|$ and density, n_e, being perpendicular to $\underset{\sim}{B}$ in the x direction (Fig. 2a). A similar situation is seen for waves propagating perpendicular to $\underset{\sim}{B}$ near the midplane of EBT. In such a plasma, stratified perpendicular to $\underset{\sim}{B}$, the refractive indices in the z and y directions ($n_z = k_z c/\omega$, $n_y = k_y c/\omega$) are constant; and for $n_y = 0$, the refractive index along the gradients satisfies a dispersion relation of the form

$$An_x^4 + Bn_x^2 + C = 0 \tag{2}$$

where

$$A = 1 - \alpha - \beta$$

$$B = [(1 - \alpha)(1 - \beta) + (1 - \alpha - \beta)]n_z^2 - [(1 - \alpha)(1 - \alpha - \beta) + (1 - \alpha)^2 - \beta]$$

$$C = (1 - \alpha)[(1 - \beta)n_z^4 - 2(1 - \alpha - \beta)n_z^2 + (1 - \alpha)^2 - \beta]$$

A resonance ($n_x^2 \to \infty$) occurs in the extraordinary mode branch at the upper hybrid frequency ($\alpha + \beta = 1$) for arbitrary values of n_z^2. Cutoffs ($n_x \to 0$) occur at the values of density such that $\alpha = 1$ and at $\alpha = (1 \pm \sqrt{\beta})(1 - n_z^2)$. The cutoff $\alpha = 1$ is associated with the ordinary mode, the cutoff $\alpha = (1 - \sqrt{\beta})(1 - n_z^2)$ is associated with the extraordinary mode, whereas the cutoff at $\alpha = (1 + \sqrt{\beta})(1 - n_z^2)$ is in the ordinary or extraordinary mode branch according to whether $\alpha < 1$ or $\alpha > 1$, respectively. Figure 3a shows typical extraordinary mode rays injected from the low and high magnetic field region. In the cold plasma theory, a wave propagating toward the cyclotron resonance from the high field

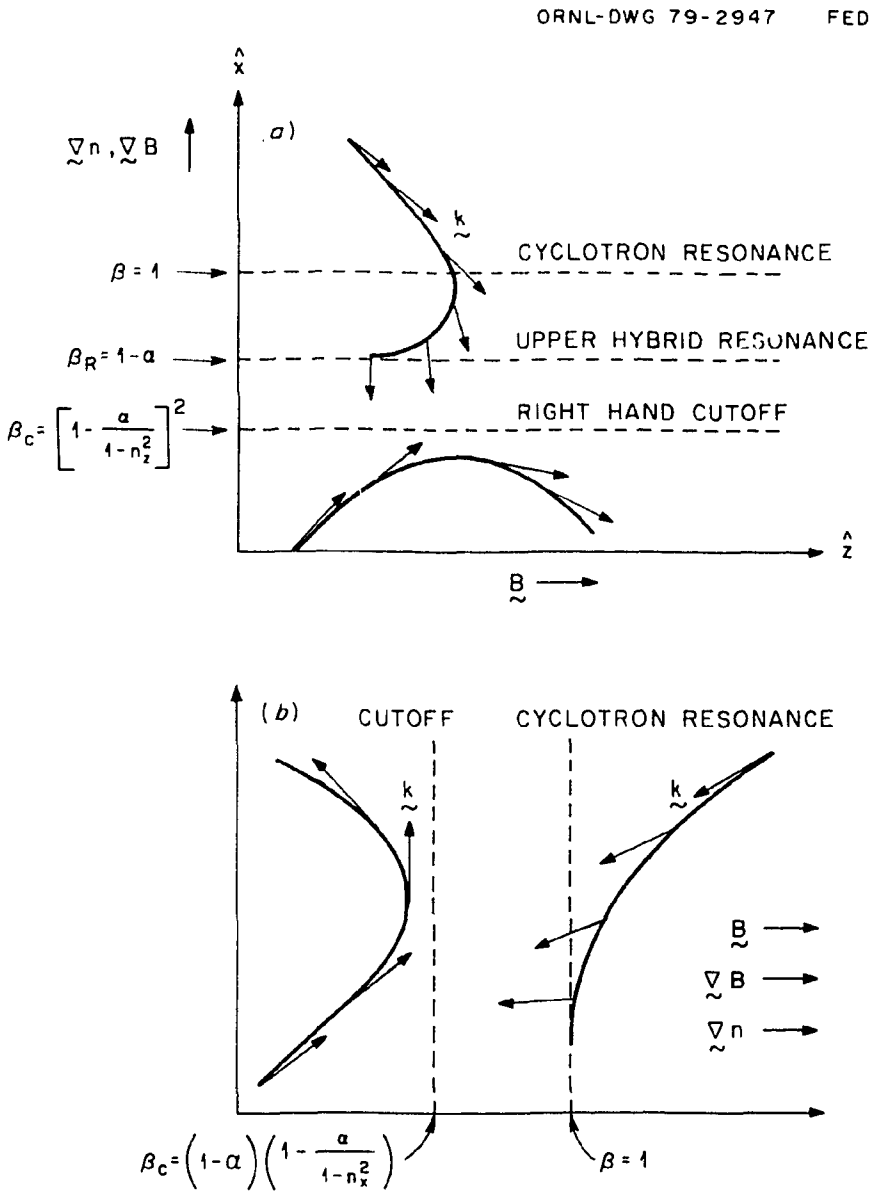
ORNL-DWG 79-2947 FED
(a)
$\nabla n, \nabla B$
$\beta = 1$
$\beta_R = 1-\alpha$
$\beta_c = \left[1 - \frac{\alpha}{1-n_z^2}\right]^2$
CYCLOTRON RESONANCE
UPPER HYBRID RESONANCE
RIGHT HAND CUTOFF
k
B
(b)
CUTOFF
CYCLOTRON RESONANCE
$\beta_c = \left(1-\alpha\right)\left(1 - \frac{\alpha}{1-n_x^2}\right)$
$\beta = 1$

Fig. 3

side passes without impediment through the cyclotron resonance to the upper hybrid resonance, where it must be absorbed or mode converted. Cyclotron absorption in a perpendicularly stratified plasma is entirely a finite temperature effect.

In other devices such as bumpy tori, mirror machines, or multipoles, the variations in B and n_e along the magnetic field are very important and in some regions can dominate variations perpendicular to $\underset{\sim}{B}$. For example, near the fundamental cyclotron resonance in EBT, particularly at the magnetic axis, the magnetic field varies strongly along the field lines (magnetic beach). As a simple model of this type of geometry, consider a plasma slab which is stratified parallel to the magnetic field (Fig. 3b). The magnetic field is taken along z, and the field strength and possibly the density are assumed to vary only with z[$\underset{\sim}{B} = B(z)\hat{z}$].

In this geometry the components of the refractive index in the x and y directions are fixed and we can, without loss of generality, choose $n_y = 0$. Using cold plasma wave theory, one finds that the parallel index of refraction n_z satisfies a dispersion relation of the form

$$An_z^4 + Bn_z^2 + C = 0 \tag{3}$$

where

$$A = (1 - \alpha)(1 - \beta)$$

$$B = -2(1 - \alpha)(1 - \alpha - \beta) - [(1 - \alpha)(1 - \beta) + 1 - \alpha - \beta]n_x^2$$

$$C = (1 - \alpha - \beta)n_x^4 - [(1 - \alpha)(1 - \alpha - \beta) + (1 - \alpha)^2 - \beta]n_x^2$$

$$+ (1 - \alpha)[(1 - \alpha)^2 - \beta]$$

Here the extraordinary mode resonance ($A \to 0$) occurs at the cyclotron layer $\beta = \omega_e^2/\omega^2 = 1$ independent of n_x, and the extraordinary mode cutoff ($C \to 0$) occurs at

$$(1 - \alpha)^2 - \beta - (1 - \alpha - \beta)n_x^2 = 0 \tag{4}$$

Figure 3b shows typical extraordinary mode rays launched toward the cyclotron resonance in a parallel stratified plasma from both the low and high magnetic field sides. As the ray approaches the resonance from the high field side, the wave vector $\underset{\sim}{k}$ turns parallel to $\underset{\sim}{B}$, the parallel phase velocity c/n_z becomes slow, and the large numbers of resonant particles produce very strong cyclotron damping.

3. THE FINITE TEMPERATURE DISPERSION RELATION AND PROPERTIES OF THE SOLUTIONS

In the present work the energy deposition was calculated by integrating the imaginary part of the refractive index along a ray path,

$$P(s) = P_0 \exp\left\{ - \int_{s_0}^{s} ds' \, \underset{\sim}{k}_i \cdot \underset{\sim}{v}_g / |\underset{\sim}{v}_g| \right\} \tag{5}$$

where

$P(s)$ = power flux density along the ray

P_0 = initial power flux density

s = path length along the ray

$\underset{\sim}{k}_i$ = imaginary part of the wave vector

$\underset{\sim}{v}_g$ = group velocity

The imaginary part of $\underset{\sim}{k}$ is obtained by solving a finite temperature dispersion relation of the form

$$D[\underset{\sim}{k},\omega,\omega_{pe}(\underset{\sim}{x}),\Omega_e(\underset{\sim}{x}),v_e] = \det[\underset{\approx}{D}] = 0 \tag{6}$$

where

$$\underset{\approx}{D} = \left(1 - \frac{c^2k^2}{\omega^2}\right)\underset{\approx}{I} + \frac{c^2}{\omega^2}\,\underset{\sim}{k}\underset{\sim}{k} + \frac{4\pi i}{\omega}\,\underset{\approx}{\sigma}$$

$\underset{\approx}{\sigma}$ = warm plasma conductivity tensor

General expressions for the conductivity tensor can be found in the literature [18,19]. However, for the present purposes the electron distribution function can be taken to be an isotropic, nonrelativistic

Maxwellian and the ion contribution can be neglected entirely. A typical element of the conductivity tensor is of the form

$$\sigma_{11} = -\frac{i}{4\pi}\frac{\omega_{pe}^2}{k_z v_e}\sum_{\ell=-N}^{N}\frac{\ell^2}{b} I_\ell(b)e^{-b} Z(\xi_\ell) \tag{7}$$

where

$$Z(\xi_\ell) = \frac{1}{\sqrt{\pi}}\int_{-\infty}^{\infty} dx \frac{e^{-x^2}}{x - \xi_\ell} = \text{plasma dispersion function}$$

$$\xi_\ell = \frac{\omega - \ell\Omega_e}{k_z v_e}$$

$$v_e = (2T_e/m_e)^{1/2}$$

$$b = k_x^2 v_e^2/2\Omega_e^2 = k_x^2\rho_e^2/2$$

$I_\ell(b)$ = modified Bessel function of order ℓ

No small argument expansion is made on the $I_\ell(b)$, and the sum is taken over all cyclotron harmonics of interest (typically N = 2). For the plasma parameters found in EBT, the energy confinement time $\tau_E \sim$ 2-5 msec is much longer than the electron-electron collision time $\nu_{ee}^{-1} \sim 10^{-4}$ sec and each particle spends only a short time in the resonance zone. Therefore, the assumption of an isotropic Maxwellian distribution for the toroidal core electrons is justified.

In many cases, useful approximation to k_i can be obtained by expanding the dispersion relation about the cold plasma roots [14,19]. Assuming $k_x^2\rho_e^2 \ll 1$, $\xi_\ell \gg 1$ for $\ell \neq 1$, and taking the large argument limit

of $Z(\xi_\ell)$ for $\ell \neq 0$ give a dispersion relation valid near the fundamental cyclotron resonance ($\omega \sim \Omega_e$) of the form

$$D = \sigma D_0(\omega,\underset{\sim}{n},\omega_{pe},\Omega_e) + D_1(\omega,\underset{\sim}{n},\omega_{pe},\Omega_e) + \xi_1 Z(\xi_1) D_2(\omega,\underset{\sim}{n},\omega_{pe},\Omega_e) \tag{8}$$

where

$$\sigma = \frac{1}{2}\frac{\omega_{pe}^2}{\omega^2}\frac{1}{n_z}\frac{c}{v_e} Z(\xi_1)$$

and D_0, D_1, D_2 are fourth degree polynomials in $\underset{\sim}{n} = c\underset{\sim}{k}/\omega$. For propagation not along field lines ($n_z \lesssim 1$) in nonrelativistic plasma ($v_e/c \ll 1$) of sufficiently high density, the quantity σ is large near $\omega = \Omega_e$

$$|\sigma(\omega = \Omega_e)| = \frac{\sqrt{\pi}}{2}\frac{\omega_{pe}^2}{\Omega_e^2}\frac{c}{v_e}\frac{1}{n_z} \gg 1 \tag{9}$$

To lowest order, n is given by

$$D_0(\omega = \Omega_e,\underset{\sim}{n}^0) = n_x^{02}n^{02} - [2(1-\alpha)n^{02} + n_x^{02}] + (1-\alpha)(2-\alpha) = 0 \tag{10}$$

where $n^{02} = n_x^{02} + n_z^{02}$. Equation (10) coincides exactly with the cold plasma dispersion relation [Eq. (2) or (3)] evaluated at $\omega = \Omega_e$ and can be solved either for $n_x^{02}(\alpha,n_z)$, $n_z^{02}(\alpha,n_x)$, or $n^{02}(\alpha,\theta)$. In any case a quadratic equation is obtained which yields two roots corresponding to the cold plasma ordinary and extraordinary modes. The first order correction is obtained by regarding D_0, D_1, D_2 as slowly varying functions of Ω_e near the resonance and expanding Eq. (9) about n^0

$$D(\underset{\sim}{n}^0 + \underset{\sim}{n}^1) = \sigma \left[D_0(\underset{\sim}{n}^0) + \underset{\sim}{n}^1 \cdot \frac{\partial}{\partial \underset{\sim}{n}} \cdot D_0(\underset{\sim}{n}^0) \right] + D_1(\underset{\sim}{n}^0) + \xi_1 Z(\xi_1) D_2(\underset{\sim}{n}^0) = 0 \tag{11}$$

Finally we get an expression for $\underset{\sim}{n}_i$ of the form

$$\underset{\sim}{n}_i \cdot \frac{\partial I_0}{\partial \underset{\sim}{n}_0} = -2 \frac{\Omega_e^2}{\omega_{pe}^2} n_z \frac{v_e}{c} D_1(\underset{\sim}{n}^0) \operatorname{Im}\left\{ \frac{1}{Z\left(\frac{\omega - \Omega_e}{k_z^0 v_e} \right)} \right\} \tag{12}$$

This approximation or similar ones have been used in a number of previous papers to evaluate cyclotron damping in tokamaks. The qualitative properties of cyclotron absorption can be summarized as follows: near the fundamental resonance, damping of the extraordinary mode is very heavy ($k_i/k_r \sim 1$) for propagation nearly parallel to the magnetic field ($\theta \sim 0$) but then decreases with increasing θ. The damping increases with increasing temperature but decreases as the density is increased. The ordinary mode is weakly damped ($k_i/k_r \sim T_e/mc^2$) in comparison to the extraordinary mode, but the damping increases with increasing θ, with increasing temperature, and with increasing density. Near the second harmonic ($\omega \sim 2\Omega_e$) both modes are weakly damped [$k_i/k_r \sim T_e/mc^2$ for extraordinary mode, $k_i/k_r \sim (T_e/mc^2)^2$ for ordinary mode] with absorption increasing as temperature and density increase. The damping of the extraordinary mode increases with θ, whereas damping of the ordinary mode peaks at an oblique angle $0 < \theta < \pi/2$.

The approximate method described above is usually adequate for high density tokamaks or other nearly perpendicularly stratified plasmas. In such cases, the cold plasma extraordinary mode resonance is in n_x

(rather than n_z) and occurs at a value of Ω_e well separated from $\Omega_e = \omega$. At the cyclotron resonance n_z remains small ($n_z \lesssim 1$) so that the inequality in Eq. (9) is satisfied. However, in EBT or a nearly parallel stratified plasma, n_z becomes large at the cold plasma resonance (in this case $\Omega_e \sim \omega$ at the cold plasma resonance) and Eq. (9) fails. Application of the weak damping expansion in such cases gives incorrect damping rates, including nonphysical absorption on the low field side of the right-hand cutoff. In order to deal with these difficulties, we use the full finite temperature dispersion tensor in our studies and obtain solutions of the dispersion relation by numerical root finding techniques.

The formulation of cyclotron absorption in terms of a homogeneous plasma, nonrelativistic dispersion relation also breaks down for waves propagating nearly perpendicular to the magnetic field ($\theta \cong \pi/2$). In that case, resonance broadening processes other than the thermal Doppler broadening described by $Z(\xi)$ must be included. Relativistic broadening is important for $n_z \lesssim v_e/c$ [14,20], and broadening due to magnetic field inhomogeniety becomes important for $n_z < (c/v)(k_\perp L)^{-1}$ where $L = (d \ln B/dx)^{-1}$ is the magnetic field scale length [15]. In either case the effect is to give nonzero absorption of the extraordinary mode and to limit the local damping rate of the ordinary mode at perpendicular propagation. We have not included these corrections in our calculations because the geometry of the cyclotron resonant surface in EBT is such that propagation perpendicular to $\underline{B}$ at resonance is very difficult to achieve (Fig. 2) and the absorption of such waves is not expected to play an important role.

A difficulty which arises in our method of calculating the power absorption (i.e., integrating k_i along a ray) is that the direction of $\underset{\sim}{k}_i$ is not determined by the ray equations for arbitrary plasma geometry. For example, in a uniform plasma the direction of $\underset{\sim}{k}_i$ is determined by the boundary conditions or the geometry of the wave launching structure and is not, in general, parallel to $\underset{\sim}{k}_r$. However, using Poynting's theorem for a time invariant, anisotropic medium [21],

$$\nabla \cdot (u\underset{\sim}{v}_g) = -\underset{\sim}{E}^* \cdot \underset{\approx}{g}^H \cdot \underset{\sim}{E} \tag{13}$$

where

$$u = \frac{1}{8\pi} \underset{\sim}{E}^* \cdot \frac{\partial}{\partial\omega} (\omega \underset{\approx}{D}^H) \cdot \underset{\sim}{E} = \text{wave energy density}$$

$$\underset{\approx}{g}^H = \frac{1}{2} (\underset{\approx}{g} + \underset{\approx}{g}^+) = \text{Hermitian part of } \underset{\approx}{g}^H$$

and making the ansatz $\underset{\sim}{E}(\underset{\sim}{x},t) = \underset{\sim}{E}_0 \exp [i(\underset{\sim}{k} \cdot \underset{\sim}{x} - \omega t)]$ where $\underset{\sim}{k} = \underset{\sim}{k}_r + i\underset{\sim}{k}_i$ ($\underset{\sim}{k}_i$ is not necessarily parallel to $\underset{\sim}{k}_r$) we obtain

$$\underset{\sim}{k}_i \cdot \underset{\sim}{v}_g = \frac{\underset{\sim}{E}_0^* \cdot \underset{\approx}{g}^H \cdot \underset{\sim}{E}_0}{\underset{\sim}{E}_0^* \cdot \frac{\partial}{\partial\omega} (\omega \underset{\approx}{D}^H) \cdot \underset{\sim}{E}_0} \tag{14}$$

This indicates that the component of $\underset{\sim}{k}_i$ along the group velocity is independent of the direction chosen for $\underset{\sim}{k}_i$. Of course, this breaks down if $\underset{\sim}{k}_i$ is exactly perpendicular to $\underset{\sim}{v}_g$.

For the particular problem of interest here, Poynting's theorem in the form of Eq. (13) is not valid. This is because derivation of Eq. (13) [21] for a dissipative medium requires that $|\underset{\approx}{g}^H| \ll |\underset{\approx}{g}^A|$, whereas near a

cyclotron harmonic in a dense plasma, we have $|\underset{\sim}{g}^H| \gg |\underset{\sim}{g}^A|$. However, even near a cyclotron harmonic a result similar to Eq. (14) can be obtained from the dispersion relation, Eq. (8), provided the absorption is not too large. Noting that in Eq. (8) $D_0(\underset{\sim}{n},\omega = \Omega_e) = 0$ is the cold plasma dispersion relation evaluated at $\omega = \Omega_e$, we see that

$$\left.\frac{\partial D_0}{\partial \underset{\sim}{n}_0} = \frac{\omega}{c}\frac{\partial D_0}{\partial \underset{\sim}{k}}\right]_{\underset{\sim}{k}=\omega\underset{\sim}{n}_0/c} = -\left.\frac{\omega}{c}\frac{\partial D_0}{\partial \omega}\right]_{\underset{\sim}{k}=\omega\underset{\sim}{n}_0/c} \underset{\sim}{v}_g \tag{15}$$

where $\underset{\sim}{v}_g$ is the group velocity at resonance as determined from cold plasma theory. Therefore, Eq. (12) becomes

$$\underset{\sim}{k}_i \cdot \underset{\sim}{v}_g = 2\,\frac{\Omega_e^2}{\omega_{pe}^2}\,\frac{k_z^0 v_e}{c}\,\frac{D_1(\underset{\sim}{n}^0)}{\dfrac{\partial D_0}{\partial \omega}}\,\mathrm{Im}\left\{\frac{1}{Z\left(\dfrac{\omega - \Omega_e}{k_z^0 v_e}\right)}\right\} \tag{16}$$

which again shows that the component of $\underset{\sim}{k}_i$ along $\underset{\sim}{v}_g$ is independent of the choice of direction for $\underset{\sim}{k}_i$.

In order to study this situation in somewhat more detail, we have obtained numerical solutions of the full dispersion relation Eq. (6) with $\underset{\sim}{k}_i$ at an arbitrary angle with respect to $\underset{\sim}{k}_r$. We find that $\underset{\sim}{k}_i \cos\psi$, where ψ is the angle between $\underset{\sim}{k}_i$ and $\underset{\sim}{v}_g$, is independent of ψ even for fairly heavily damped waves. Figure 4 shows the magnitude of k_i and $k_i \cos\psi$ plotted for the extraordinary mode as a function of ψ at the cyclotron resonance, $\Omega_e/\omega = 1$. For the case shown the parameters were $\omega/2\pi = 18$ GHz, $\omega_{pe}^2/\omega^2 = 0.7$, $v_e/c = 0.034$. The angle θ between $\underset{\sim}{k}_r$ and $\underset{\sim}{B}$ was 27.7°, and the angle ϕ between $\underset{\sim}{v}_g$ and $\underset{\sim}{B}$ was 83.7°. Despite the heavy damping [$k_i(\psi = 0) = 0.32$/cm] we see that $\underset{\sim}{k}_i \cos\psi$ is virtually constant.

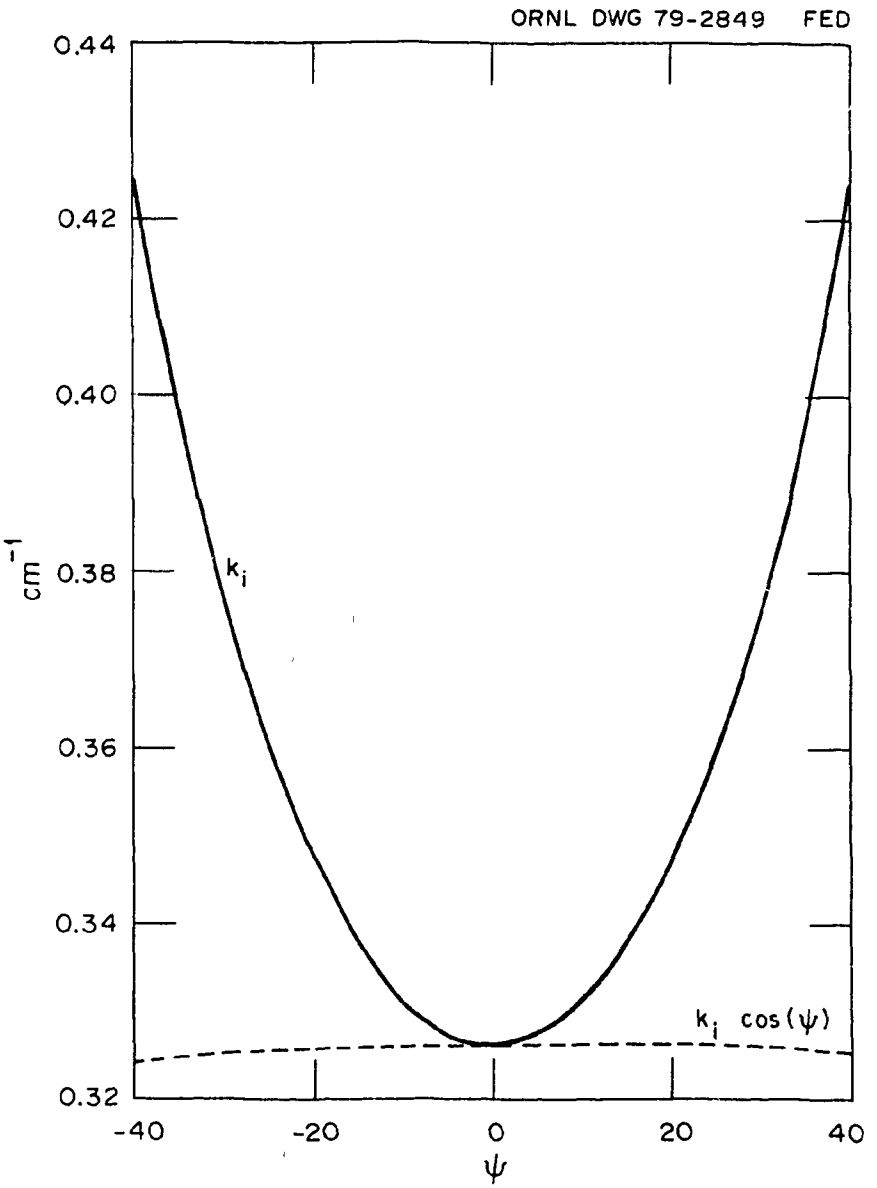
ORNL DWG 79-2849 FED
0.44
0.42
0.40
0.38
0.36
0.34
0.32
cm⁻¹
k_i
$k_i \cos(\psi)$
-40
-20
0
20
40
ψ

Fig. 4

For fixed ω, the shape of the absorption line (i.e., k_i considered as a function of Ω_e) depends strongly on the plasma geometry. In a perpendicularly stratified plasma, k_z is fixed and real. The resonance absorption line is approximately Gaussian shaped and is described accurately by the approximation given by Eq. (12), provided $\omega_{pe}^2 c/\Omega_e^2 v_e \gg 1$. Absorption line calculations for parameters typical of tokamaks are presented in Ref. [14].

However, if the geometry is such that k_z develops a finite imaginary part in the resonance region, the extraordinary mode line shape will be distorted from Gaussian. In particular, for a parallel-stratified plasma, k_x is fixed and real, whereas $\mathrm{Im}\{k_z\}$ becomes large near $\omega \cong \Omega_e$ so that the plasma dispersion function becomes highly oscillatory $Z(\xi) \sim i\sqrt{\pi}\exp(-\xi^2)$. Also, since $|k_z| \to 0$ at the cutoff region and $k_z = 0$ is an essential singularity of the plasma dispersion function, the dispersion relation is found to have an infinite number of roots distributed throughout the complex k_z plane in the frequency region between the right-hand cutoff and the cyclotron resonance [22]. Figure 5 shows extraordinary mode $\mathrm{Re}\{k_z\}$ and $\mathrm{Im}\{k_z\}$ plotted as a function of Ω_e/ω for $n_x = 0.6$ with plasma parameters typical of EBT-I [i.e., $\omega = 2\pi(18\ \mathrm{GHz})$, $v_e/c = 0.034$, $\omega_{pe}^2/\omega^2 = 0.3$]. Far from the fundamental cyclotron resonance, $\mathrm{Re}\{k_z\}$ agrees with cold plasma results obtained from Eq. (3) except for a small perturbation at the second harmonic resonance. When approaching resonance from the high field side, $\mathrm{Re}\{k_z\}$ peaks at $\Omega_e/\omega = 1.025$ and remains finite at $\Omega_e/\omega = 1.0$. The damping rate, $\mathrm{Im}\{k_z\}$, becomes quite large near resonance, and clearly the wave approaching from the high magnetic field side is totally absorbed. This result is virtually independent of the

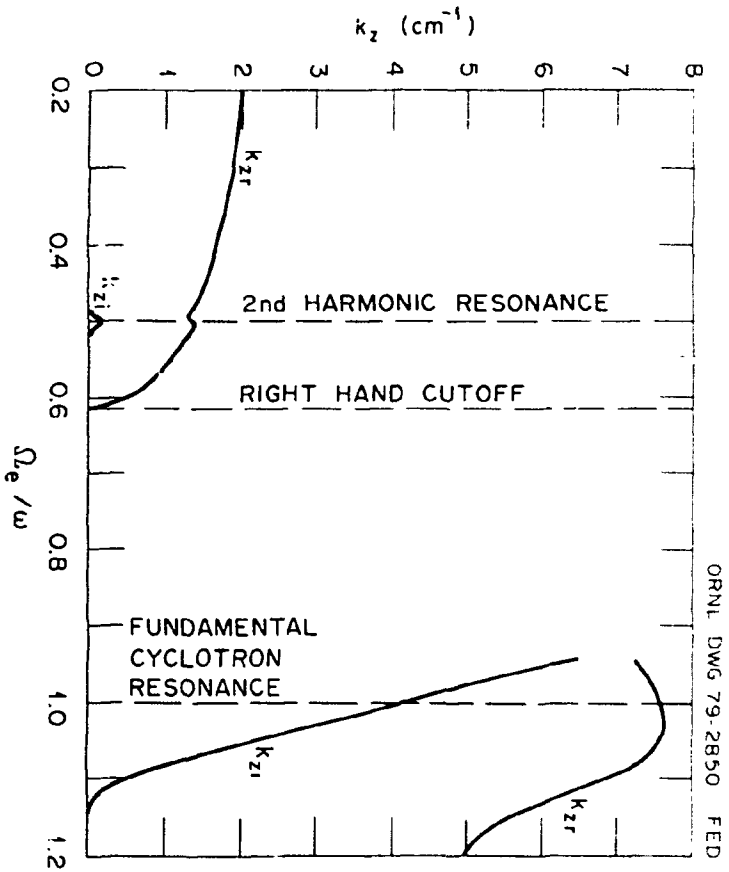
k_z (cm^{-1})
0
1
2
3
4
5
6
7
8
0.2
0.4
0.6
0.8
1.0
1.2
k_{zr}
k_{zi}
2nd HARMONIC RESONANCE
RIGHT HAND CUTOFF
FUNDAMENTAL
CYCLOTRON
RESONANCE
k_{zi}
k_{zr}
Ω_e / ω
ORNL DWG 79-2850 FED

Fig. 5

plasma density or the value of n_x. The relative weakness of second harmonic absorption is indicated by the magnitude of $\mathrm{Im}\,k_z$ at the second harmonic resonance. Between the cutoff $\omega_e/\omega = 0.61$ and resonance, the dispersion relation has multiple solutions. The roots shown in this range in Fig. 5 were obtained by continuity, following the root from the high field side.

4. FRACTIONAL ABSORPTION CALCULATIONS FOR PLANE-STRATIFIED PLASMAS

Because of the complicated EBT geometry, the fraction of power absorbed from a propagating ray depends sensitively on the initial position of the ray and injection angle. In order to obtain a qualitative understanding of the relative importance of the different modes, geometrical characteristics, and plasma parameters, we have compiled a compendium of calculations of fractional absorbed power as rays pass through fundamental and second harmonic cyclotron resonances in plane-stratified plasmas having parameters appropriate for EBT devices. For consideration of EBT-I the parameters are taken to be $\omega/2\pi$ = 18 GHz, T_e = 300 eV [this corresponds to $v_e/c = (2T_e/mc^2)^{1/2} = 0.034$], and ω_{pe}^2/ω^2 = 0.3, 0.5, 0.7 (this corresponds to n_e = 1.2, 2.0, 2.8 $\times$ 10^{12} cm^{-3}, respectively). In order to gain some understanding of the implications for hotter, denser devices, we have also performed calculations for a projected EBT-II device [23] with parameters $\omega/2\pi$ = 120 GHz, T_e = 2 keV (corresponding to v_e/c = 0.09) and ω_{pe}^2/ω^2 = 0.3, 0.5, 0.7 (corresponding to n_e = 5.4 $\times$ 10^{13} cm^{-3}, 8.9 $\times$ 10^{13} cm^{-3}, and 1.25 $\times$ 10^{14} cm^{-3}, respectively).

Calculations were performed for the ordinary mode in a parallel-stratified plasma with linearly increasing magnetic field, $\underset{\sim}{B}(\underset{\sim}{x}) = B_0(1 + z/L)\hat{z}$. As mentioned previously, the extraordinary mode is completely absorbed in this geometry when launched from the high magnetic field side. The magnetic scale length L was taken to be 10 cm in the calculations for both EBT-I and EBT-II. This value is typical of, or slightly longer than, magnetic gradient scale lengths at the fundamental cyclotron resonance in EBT-I (Fig. 1). For EBT-II, scale lengths may be somewhat

larger, so that these results represent minimum absorption for EBT-II. For comparison we also evaluated ordinary and extraordinary modes in a perpendicularly stratified plasma with linearly increasing magnetic field, $\underset{\sim}{B}(\underset{\sim}{x}) = B_0(1 + x/L)\hat{z}$. Again L was taken to be 10 cm. The fraction of power absorbed, f, is calculated by actually tracing rays in the appropriate plasma geometry and integrating k_i,

$$f = 1 - \exp\left[-2\int_{s_1}^{s_2} ds\ k_i(s)\right] \tag{17}$$

where $\underset{\sim}{k}_i(s)$ is chosen to be parallel to the local group velocity $\underset{\sim}{v}_g(s)$ and s is the arc length along a ray.

Figure 6 shows the fraction of power absorbed for typical EBT-I parameters. Figure 6(a) is for the ordinary mode in a parallel-stratified plasma as a function of the perpendicular index of refraction n_x with which the ray is injected. It can be seen that the fractional absorption increases with density and with angle of propagation relative to the magnetic field. The absorption increases rapidly with n_x because the magnitude of k_i increases with n_x, and increasing n_x causes the ray to spend a longer time in the resonant zone. However, the finite radial size of EBT-I and the curvature of the resonant zone (i.e., deviation from plane stratification) limit the per pass fractional absorption for ordinary mode radiation to <1%, even for nearly perpendicularly propagating rays in the actual device. Over most of the spectrum in n_x, f is less than 10^{-3}. Figures 6b and 6c, respectively, show ordinary mode absorption and extraordinary mode absorption in perpendicularly stratified plasma as a function of the parallel index of refraction n_z with which

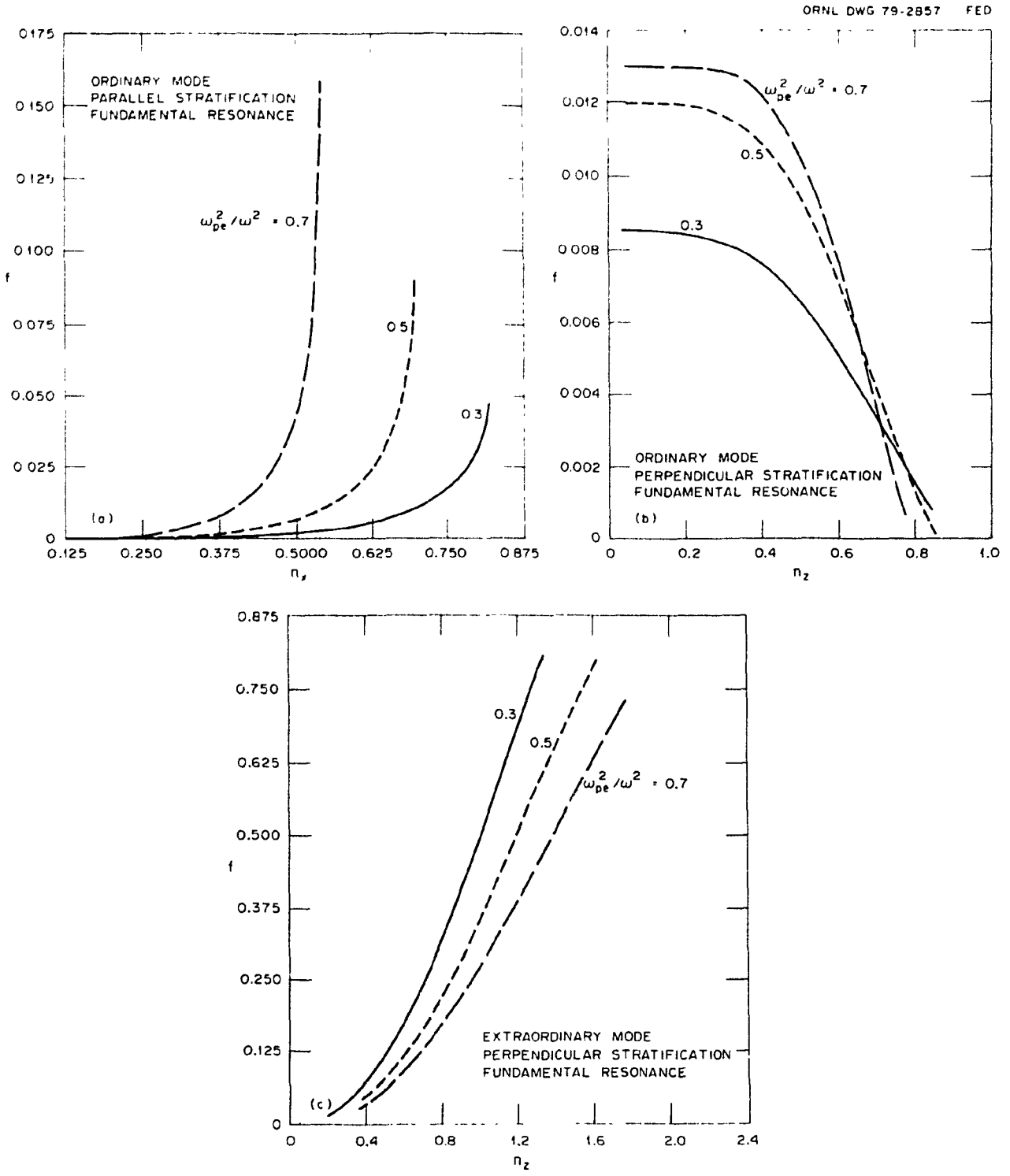
ORNL DWG 79-2857 FED
ORDINARY MODE
PARALLEL STRATIFICATION
FUNDAMENTAL RESONANCE
$\omega_{pe}^2/\omega^2 = 0.7$
0.5
0.3
(a)
f
n_x
ORDINARY MODE
PERPENDICULAR STRATIFICATION
FUNDAMENTAL RESONANCE
(b)
n_z
EXTRAORDINARY MODE
PERPENDICULAR STRATIFICATION
FUNDAMENTAL RESONANCE
(c)

Fig. 6

the ray is injected. This type of geometry does not actually occur for the 18-GHz fundamental resonance in EBT, although the 10.6-GHz resonance might be modeled as perpendicularly stratified near the midplane. The ordinary mode (Fig. 6b) absorption is quite small and decreases with increasing n_z. The extraordinary mode absorption (Fig. 6c) decreases with density and increases rapidly with increasing n_z. In this case, the magnitude of k_i increases as the wave vector becomes more nearly parallel to $\underset{\sim}{B}$, and the ray stays longer in the resonant zone as n_z increases.

Figure 7 shows similar plots of fractional power absorption for the projected EBT-II parameters. The important point here is that for a hotter, denser plasma such as EBT-II, the ordinary mode is quite heavily absorbed for both directions of stratification.

Figure 8 shows fractional absorption at the second harmonic resonance for parameters characteristic of the toroidal core plasma in EBT-I. In Figs. 8a and 8b is plotted the second harmonic absorption for the ordinary mode in parallel and perpendicularly stratified geometry, respectively; Figs. 8c and 8d have similar plots for the extraordinary mode. For fixed density in parallel stratification, the fractional absorption f increases with n_x. The obtainable absorption is bounded, however, because the waves do not propagate for n_x above the limiting values

$$n_x^2 = 1 - \alpha \qquad \text{(ordinary mode)}$$

$$n_x^2 = \frac{(1 - \alpha)^2 - \beta}{1 - \alpha - \beta} \qquad \text{(extraordinary mode)}$$

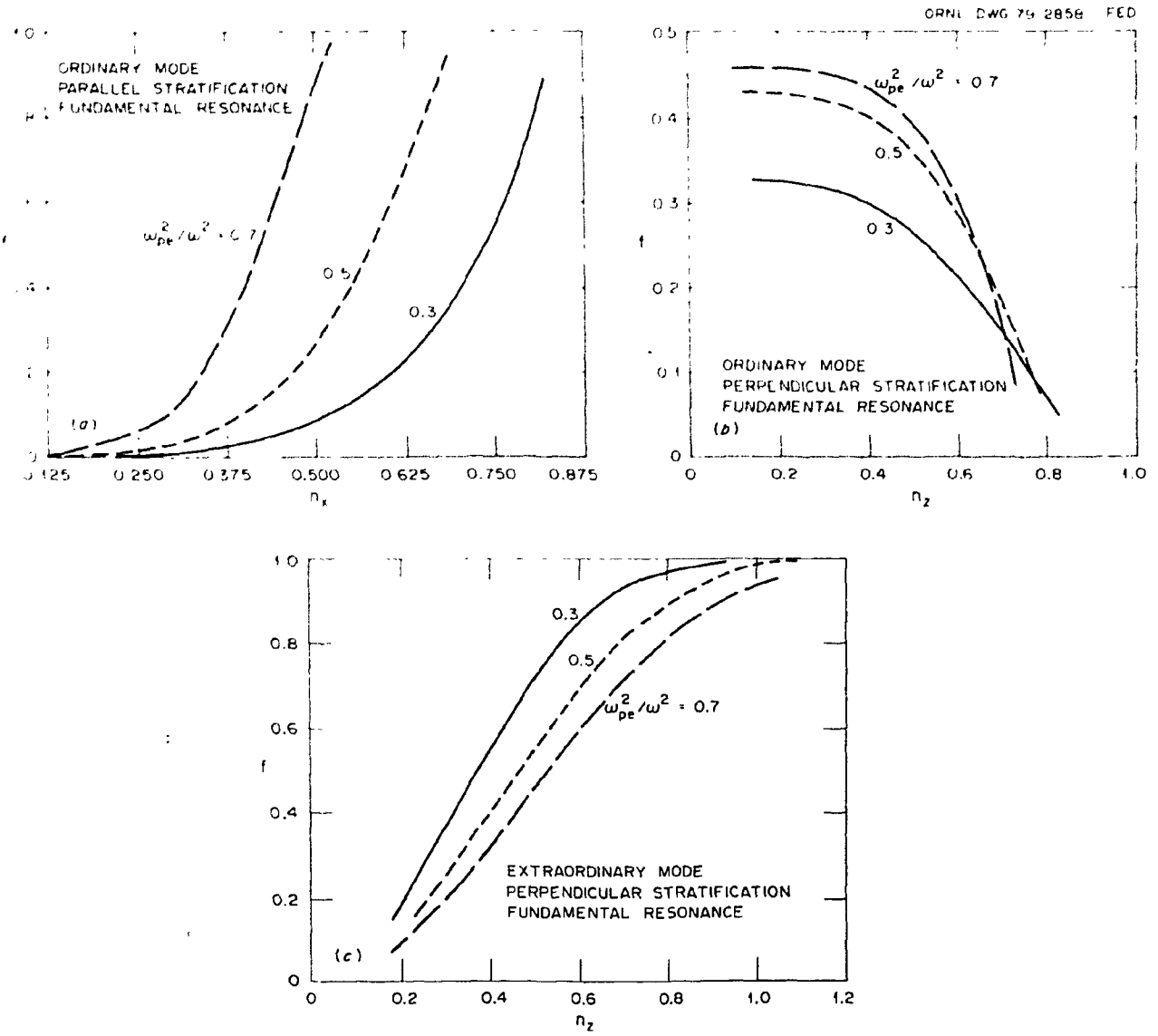
ORNL DWG 79 2858 FED
ORDINARY MODE
PARALLEL STRATIFICATION
FUNDAMENTAL RESONANCE
$\omega_{pe}^2/\omega^2 = 0.7$
0.5
0.3
(a)
0.125 0.250 0.375 0.500 0.625 0.750 0.875
n_x
$\omega_{pe}^2/\omega^2 = 0.7$
0.5
0.3
ORDINARY MODE
PERPENDICULAR STRATIFICATION
FUNDAMENTAL RESONANCE
(b)
0 0.2 0.4 0.6 0.8 1.0
n_z
0.3
0.5
$\omega_{pe}^2/\omega^2 = 0.7$
EXTRAORDINARY MODE
PERPENDICULAR STRATIFICATION
FUNDAMENTAL RESONANCE
(c)
0 0.2 0.4 0.6 0.8 1.0 1.2
n_z

Fig. 7

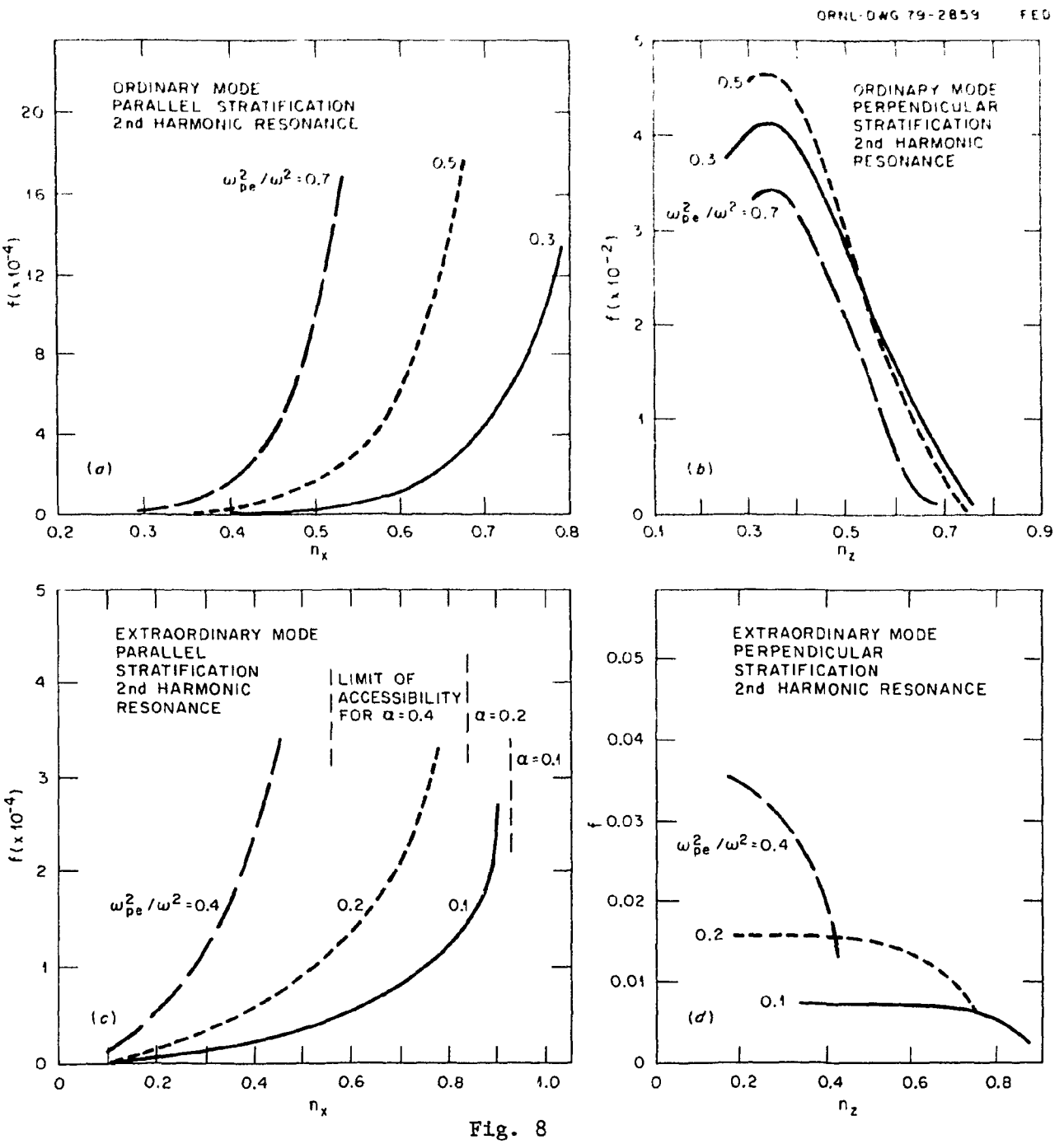
ORNL-DWG 79-2859 FED
ORDINARY MODE
PARALLEL STRATIFICATION
2nd HARMONIC RESONANCE
$\omega_{pe}^2/\omega^2=0.7$
0.5
0.3
(a)
$f(\times10^{-4})$
n_x
ORDINARY MODE
PERPENDICULAR
STRATIFICATION
2nd HARMONIC
RESONANCE
0.5
0.3
$\omega_{pe}^2/\omega^2=0.7$
(b)
$f(\times10^{-2})$
n_z
EXTRAORDINARY MODE
PARALLEL
STRATIFICATION
2nd HARMONIC
RESONANCE
LIMIT OF
ACCESSIBILITY
FOR $\alpha=0.4$
$\alpha=0.2$
$\alpha=0.1$
$\omega_{pe}^2/\omega^2=0.4$
0.2
0.1
(c)
$f(\times10^{-4})$
n_x
EXTRAORDINARY MODE
PERPENDICULAR
STRATIFICATION
2nd HARMONIC RESONANCE
$\omega_{pe}^2/\omega^2=0.4$
0.2
0.1
(d)
f
n_z

Fig. 8

From the figures we see that second harmonic absorption of the ordinary mode for these EBT-I parameters is less than $\sim 2 \times 10^{-3}$ and absorption of the extraordinary mode is less than a few percent. These results, which are confirmed by calculations in mirror geometry (Section 4), show that wave absorption at the second harmonic resonance does not play a role in heating of the core plasma in EBT-I. Figure 9 shows second harmonic absorption calculations similar to those in Fig. 8 but for the parameters characteristic of EBT-II used in Fig. 7. The results are qualitatively like those shown in Fig. 8 but the absorption is much stronger. The results for extraordinary mode (Figs. 9c and 9d) showing tens of percents wave absorption over a broad spectrum of n_x and n_z indicate that second harmonic heating of the core plasma will be important in the next generation of EBT devices.

ORNL-DWG 79-2865 FED

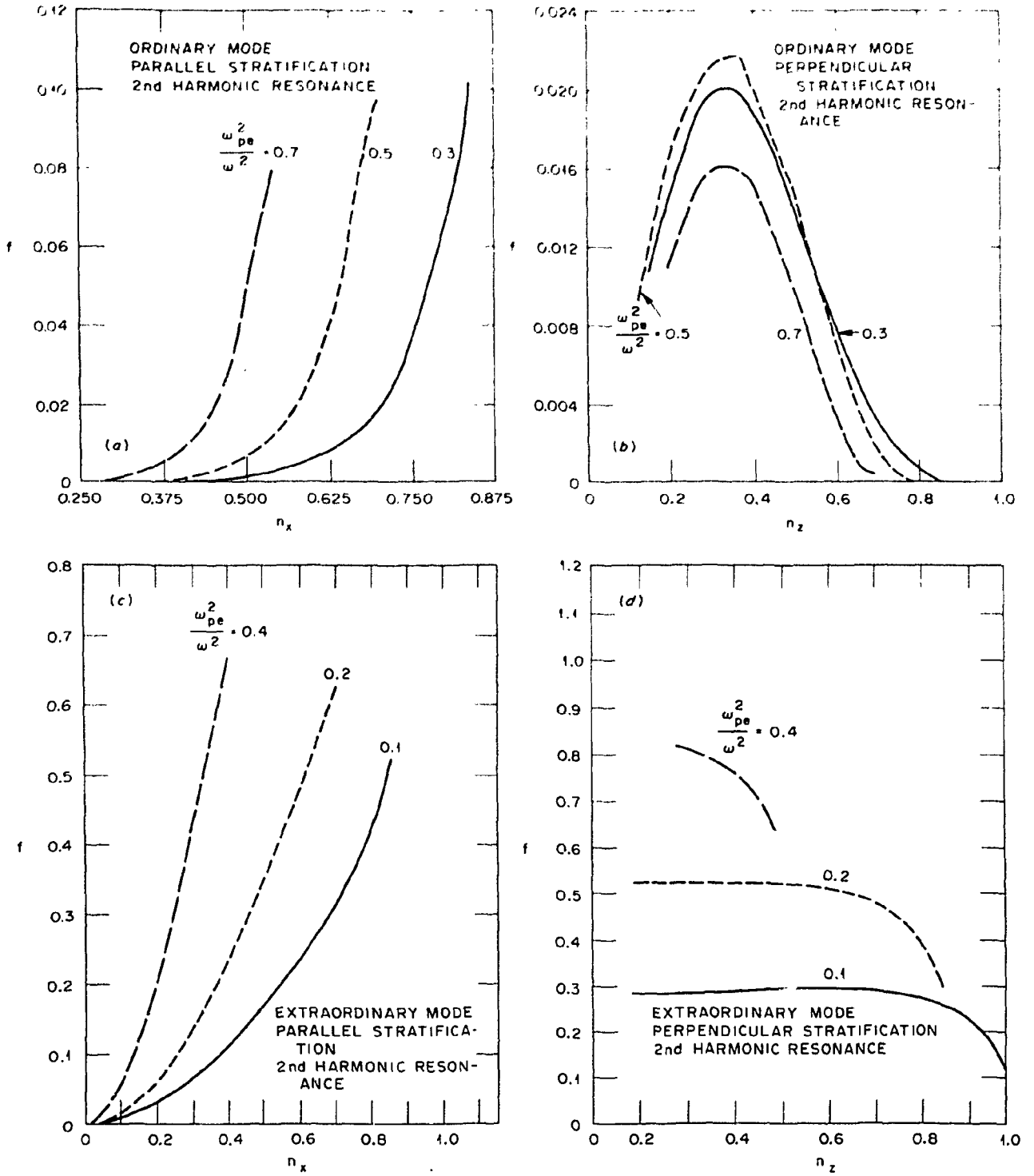

Fig. 9

5. CYCLOTRON DAMPING IN EBT GEOMETRY

We now present cyclotron damping calculations for nonstratified plasma geometry more representative of the actual EBT configuration. In particular we consider a bumpy cylinder magnetic field, $\underset{\sim}{B}(\underset{\sim}{x}) = B_z(r,z)\hat{z} + B_r(r,z)\hat{r}$, given analytically as the field due to a set of coaxial current loops spaced uniformly along the z axis [17]. A non-self-consistent density model for the low beta core plasma was adopted in which $n_e(\underset{\sim}{x})$ is constant along magnetic field lines and is an explicit function of the toroidal magnetic flux $\psi(r,z)$,

$$n_e(x) = n_0 \frac{1 - \tanh\left[\dfrac{\psi(\underset{\sim}{x}) - \psi(r_0,\ z = 0)}{\delta^2}\right]}{1 + \tanh\left[\psi(r_0,\ z = 0)/\delta^2\right]} \tag{18}$$

where

$$\psi(r,z) = \int_0^r dr'\ r' B_z(r',z)$$

Here r_0 plays the role of a plasma radius (typically $r_0 = 10$ cm, which is approximately the radius of the annulus) and δ is a gradient scale length (typically $\delta \sim 3$ cm).

The ray paths are traced using the Hamiltonian form of the geometrical optics equations [17,21]

$$\frac{d\underset{\sim}{x}}{ds} = \frac{1}{|\underset{\sim}{v}_g|}\frac{d\underset{\sim}{x}}{dt} = -\mathrm{sgn}\left(\frac{\partial D}{\partial \omega}\right)\frac{\partial D/\partial \underset{\sim}{k}}{|\partial D/\partial \underset{\sim}{k}|} \tag{19}$$

$$\frac{d\underset{\sim}{k}}{ds} = \frac{1}{|\underset{\sim}{v}_g|} \frac{d\underset{\sim}{k}}{dt} = \mathrm{sgn}\left(\frac{\partial D}{\partial \omega}\right) \frac{\partial D/\partial \underset{\sim}{x}}{|\partial D/\partial \underset{\sim}{k}|} \tag{20}$$

and using the Appleton-Hartree dispersion relation $D[\underset{\sim}{k}, \omega_{pe}(\underset{\sim}{x}), \Omega_e(\underset{\sim}{x})] = 0$, Eq. (1). The parameter s is the arc length along the ray. The ray equations Eqs. (19) and (20), as well as the wave damping equation Eq. (5), are integrated numerically from given initial conditions $\underset{\sim}{x}_0$, $\underset{\sim}{k}_0$.

Figure 10 shows the results of injecting extraordinary mode rays into the bumpy cylinder equilibrium at varying angles from two points located in the equatorial plane (y = 0). The plasma parameters were chosen to be representative of EBT-I: $\omega/2\pi$ = 18 GHz, $(\omega_{pe}/\omega)_{max}$ = 0.4, and v_e/c = 0.034. Also shown in Fig. 10 are the magnetic field lines and equatorial cross sections of the first and second harmonic resonant surfaces and the right-hand cutoff. The fraction of power absorbed in passing through resonance is indicated by each ray. A group of rays was injected from the low field region at the mirror midplane (z = 0) and outside the core plasma x = -18 cm. It can be seen that these rays do not penetrate to the cyclotron resonant surface but are reflected at the right-hand cutoff. Absorption at the second harmonic resonance, which is accessible, is negligible (<2% for the most heavily damped ray).

It is of interest to examine the fate of an extraordinary mode ray originating near the mirror throat, which, for example, might arise from depolarization of an ordinary mode ray on reflection. Figure 10 also shows ray paths and wave vectors for extraordinary mode rays injected at varying angles from a point near the mirror coil. On this side, the cyclotron resonance zone is accessible. It can be seen that the rays

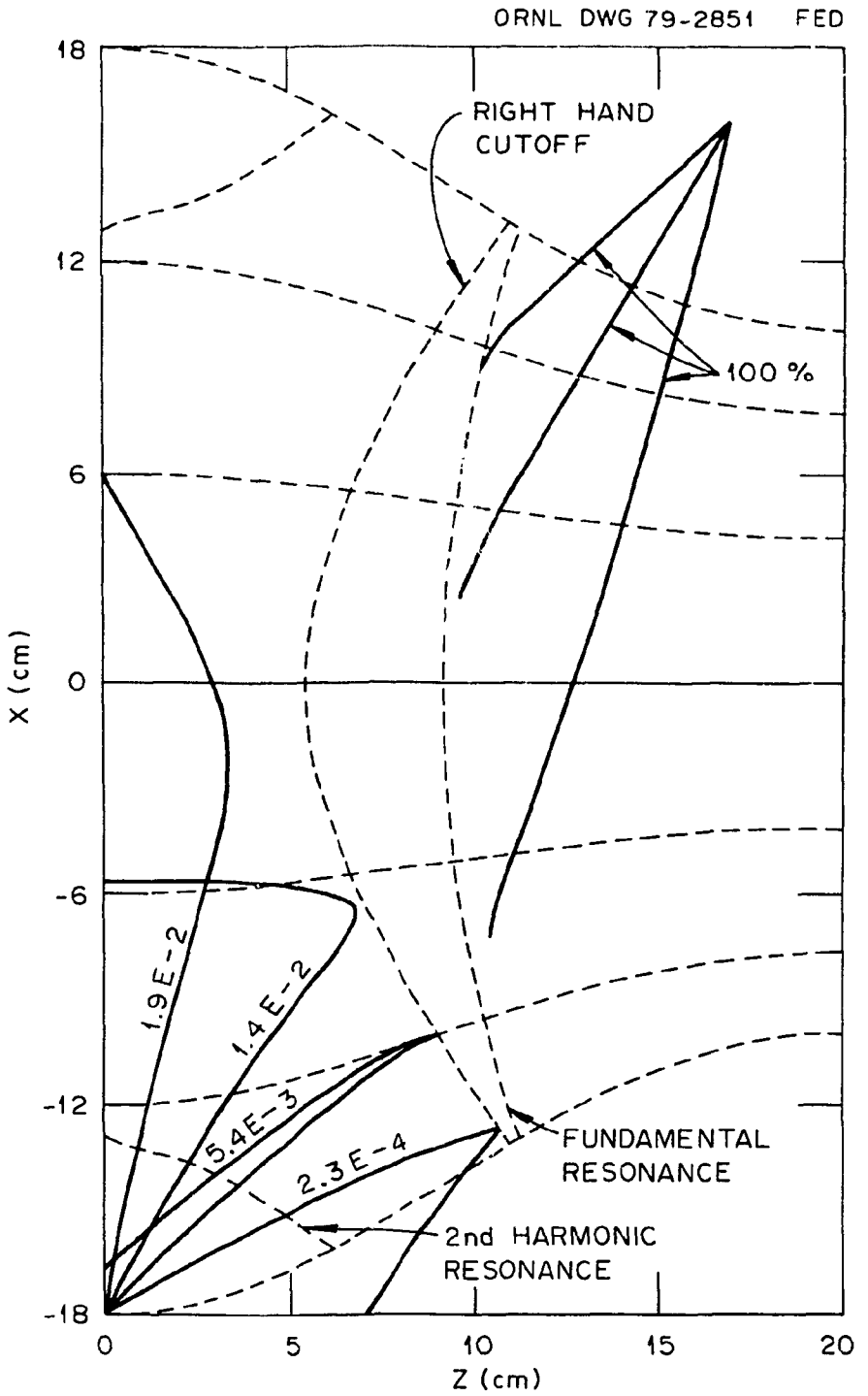
ORNL DWG 79-2851 FED
RIGHT HAND CUTOFF
100 %
1.9E-2
1.4E-2
5.4E-3
2.3E-4
FUNDAMENTAL RESONANCE
2nd HARMONIC RESONANCE
X (cm)
Z (cm)
18
12
6
0
-6
-12
-18
0
5
10
15
20

Fig. 10

approach the cyclotron resonance layer with v_g nearly perpendicular to B and k nearly parallel to B. This is characteristic of parallel-stratified media in the cold plasma model. The rays are terminated at the point at which 99% of the wave power has been absorbed. For the EBT-I parameters used in the calculation, the waves are competely damped well before reaching the resonant layer.

The situation is much less complicated for the ordinary mode. As long as the microwave frequency is higher than the plasma frequency, the entire plasma is accessible to the ordinary mode. Figure 11 shows ordinary mode rays for the same equilibrium and injection geometry as shown in Fig. 10. The rays are virtually straight, with slight curvature due to density gradients. For the EBT-I parameters used, only rays within a narrow cone have more than 1% of the wave energy absorbed in passing through the fundamental cyclotron resonance. Absorption of the ordinary mode at the second harmonic resonance is entirely negligible ($f \leq 10^{-4}$).

Similar calculations have been performed for plasmas having parameters characteristic of the projected values for EBT-II. Figure 12 shows the result of injecting extraordinary mode rays at varying angles into a plasma with $\omega/2\pi$ = 120 GHz, $(\omega_{pe}/\omega)_{max}$ = 0.4, and v_e/c = 0.09. In this case there is significant absorption ($f \sim 60\%$) at the second harmonic resonance from the rays injected near the midplane. The cross marks indicate the location at which 10%, 20%, ... of the power is absorbed. The rays injected from the high field side are again completely absorbed. Figure 13 shows the propagation and absorption of ordinary mode energy in EBT-II plasma. At this density and temperature the

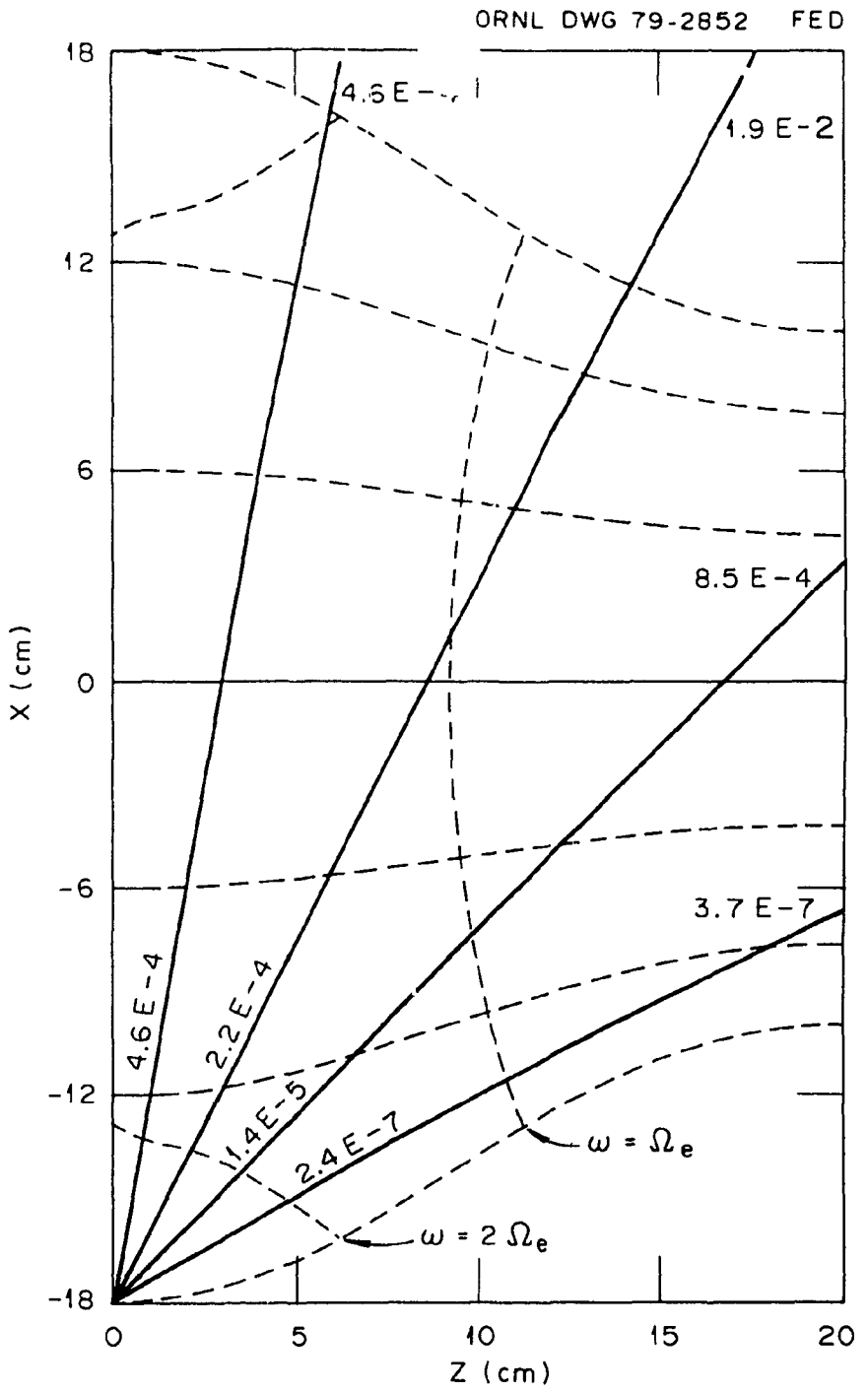
ORNL DWG 79-2852 FED
18
12
6
0
-6
-12
-18
X (cm)
0
5
10
15
20
Z (cm)
4.6 E-4
2.2 E-4
1.1 E-5
2.4 E-7
1.9 E-2
8.5 E-4
3.7 E-7
ω = Ω_e
ω = 2 Ω_e

Fig. 11

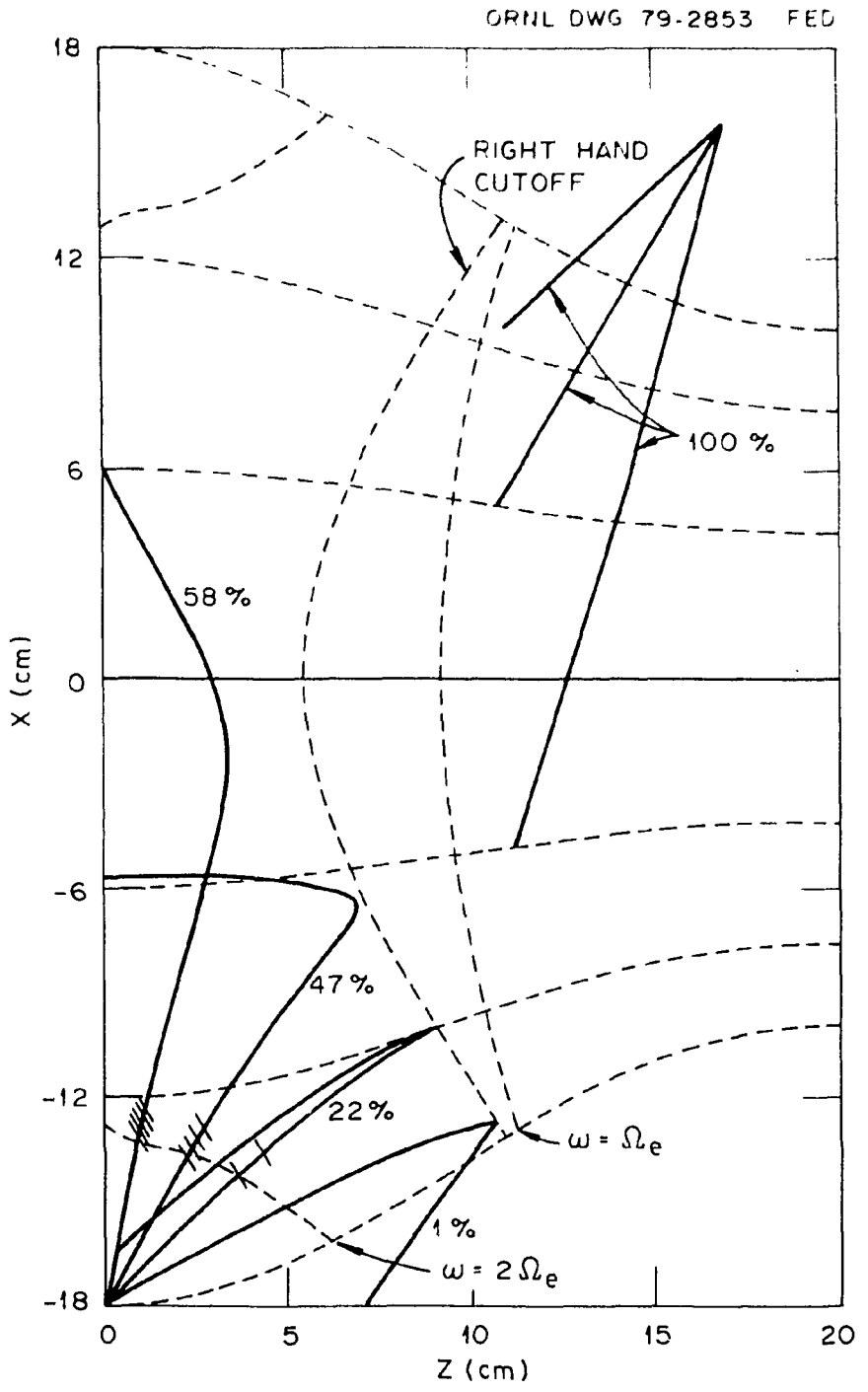
ORNL DWG 79-2853 FED
RIGHT HAND
CUTOFF
100 %
58 %
47 %
22 %
1 %
ω = Ωe
ω = 2Ωe
X (cm)
Z (cm)
18
12
6
0
-6
-12
-18
0
5
10
15
20

Fig. 12

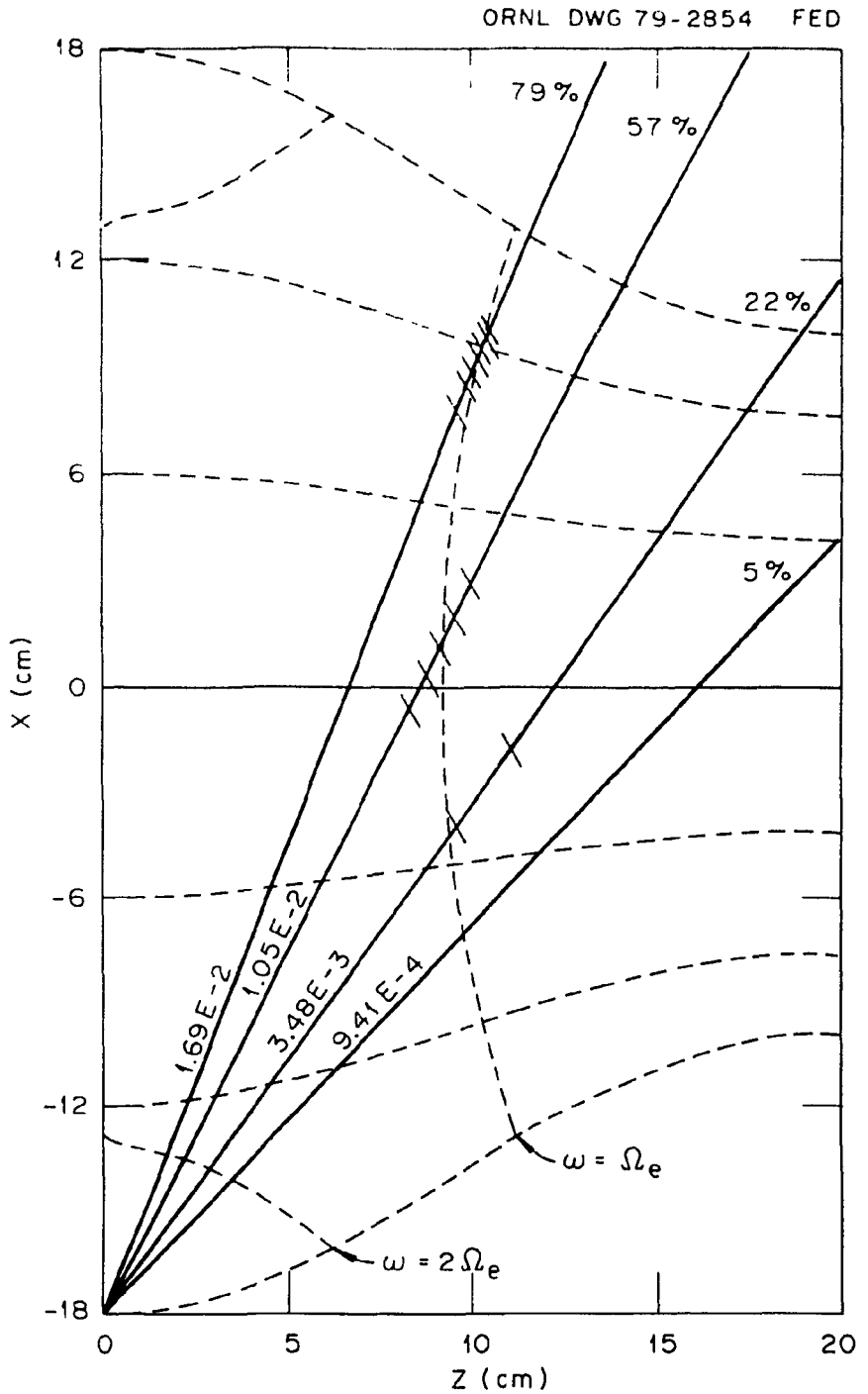
ORNL DWG 79-2854 FED
79%
57%
22%
5%
1.69E-2
1.05E-2
3.48E-3
9.41E-4
ω = Ω_e
ω = 2Ω_e
X (cm)
Z (cm)
18
12
6
0
-6
-12
-18
0
5
10
15
20

Fig. 13

ordinary mode is heavily absorbed by the core plasma ($f \lesssim 80\%$). Absorption of the ordinary mode at the second harmonic resonance is again quite small ($f \lesssim 2\%$).

6. QUALITATIVE PICTURE OF ECH IN EBT

From the cyclotron damping calculations discussed in the previous sections, certain important features of the microwave heating process in EBT can be clearly discerned. The density, temperature, and geometry of the core plasma in EBT-I are such that the direct absorption of the ordinary mode is negligibly weak. Although the extraordinary mode is totally absorbed at the fundamental cyclotron resonance if it can propagate from the high magnetic field side, this resonance is inaccessible to waves propagating from the low field (midplane) side. Heating of the core plasma at the second harmonic resonance, which is accessible, can be neglected for both ordinary and extraordinary modes.

One possiblility which has been considered to explain the strong heating of the core plasma experimentally observed in EBT-I is to include finite temperature effects in the calculation of the extraordinary mode cutoff. In a finite temperature treatment, the right-hand cutoff disappears if the density is sufficiently low and the temperature high. Physically this occurs if the resonance is thermally broadened so that large numbers of resonant particles are present at the cold plasma cutoff,

$$\left.\frac{\omega - \Omega_e}{k_\parallel v_e}\right]_{\Omega_e \text{ cutoff}} = \frac{1 - \sqrt{\beta_c}}{n_\parallel v_e/c} = \frac{\alpha}{n_\parallel v_e/c} \sim \frac{\omega_{pe}^2}{\Omega_e^2}\frac{c}{v_e} \lesssim 1 \qquad (21)$$

In the surface plasma of EBT-I ($n_e \sim 2 \times 10^{11}$, $T_e \sim 20$ eV) this parameter is $\omega_{pe}^2 c/\omega^2 v_e \sim 6$, and in the core plasma it is ~15. Thus the cutoff is also present in the finite temperature theory, even for the surface plasma where the density is low and the evanescent region is thin.

The thinness of the evanescent layer in the surface plasma (see Fig. 2) suggests that extraordinary mode energy might be absorbed and penetrate to the high field region by means of Budden tunneling [24]. This possibility was examined in detail in [25], where the Budden tunneling transmission and absorption coefficients were extended to allow an arbitrary angle of propagation in a parallel-stratified plasma. For extraordinary mode waves propagating exactly along a linearly increasing magnetic field, the Budden power and absorption and transmission coefficients, $|A|^2$ and $|T|^2$, are

$$|A|^2 = e^{-\pi k_0 z_0}\left(1 - e^{-\pi k_z z_0}\right)$$

$$|T|^2 = e^{-\pi k_0 z_0} \tag{22}$$

where

$k_0 = \frac{\omega}{c}$ = free space wave number

$z_0 = \frac{\omega_{pe}^2}{\omega^2} L$ = width of evanescent region

L = magnetic field gradient scale length

Using parameters appropriate for the surface plasma in EBT-I ($n_e \sim 1\text{-}2 \times 10^{11}/cm^3$, $L \cong 6.5$ cm), one obtains absorption and transmission coefficients

in the range $A_{/}^{2} \sim 0.02$ to 0.125 and $A^{2} \cong 0.02$ to 0.15. As shown in [25], only small deviations from these results are obtained for oblique angles of propagation up to $n_x \sim 0.5$. Budden tunneling can, therefore, make some contribution to the flow of extraordinary mode energy to the high magnetic field region and to the heating of the surface plasma.

It appears, however, that the most important mechanism by which extraordinary mode waves reach the high field region in EBT is depolarization of the ordinary mode upon reflection or scattering by a conducting wall surface [26]. When, for example, an ordinary mode wave in a magnetized plasma is incident on a perfectly conducting surface in contact with the plasma, a significant amount of power in the reflected wave is in the extraordinary mode depending on plasma density, magnetic field, and angle of incidence.

In [26] the wave depolarization situation diagrammed in Fig. 14 was investigated in detail. A perfectly conducting surface is in the x-y plane, and a uniform magnetic field $\underset{\sim}{B}$ is in the x-z plane making angle ψ with respect to the z axis. An incident wave of pure characteristic mode (for example, ordinary mode) is incident from above with refractive index $\underset{\sim}{n}^{O}$ where n_x, n_y are specified and n_z^O is determined from the Booker quartic equation [24]. For the reflected ordinary wave, n_x, n_y are conserved but $n_z = n_z^{O'}$ is, in general, different from n_z of the incident wave, and the electric field eigenvector $\underset{\sim}{E}^{O'}$ is different from the electric field of the incident ordinary mode wave $\underset{\sim}{E}^{O}$. In order to enforce the boundary condition that the transverse component of the electric field vanish at the surface, it is necessary that a component of extraordinary mode $\underset{\sim}{E}^{X'}$ be included in the reflected wave,

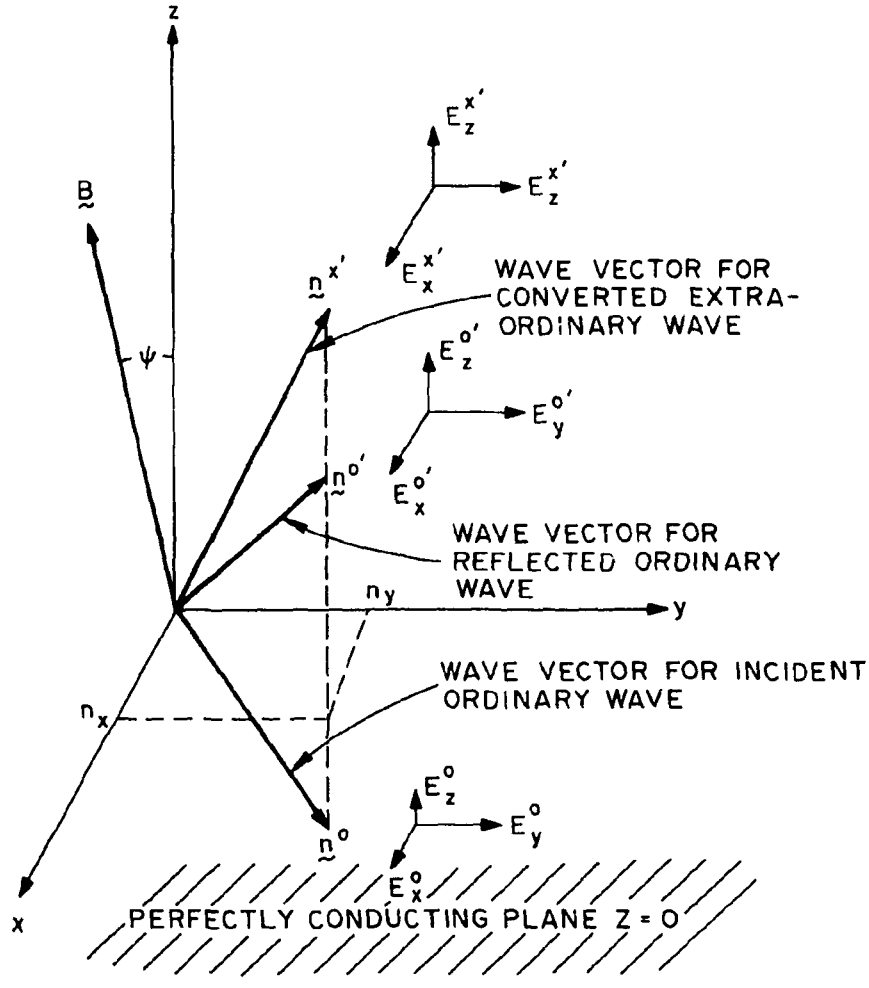
ORNL-DWG 79-2855 FED
z
B
ψ
$E_z^{x'}$
$E_z^{x'}$
$E_x^{x'}$
$n^{x'}$
WAVE VECTOR FOR CONVERTED EXTRA-ORDINARY WAVE
$E_z^{o'}$
$E_y^{o'}$
$E_x^{o'}$
$n^{o'}$
WAVE VECTOR FOR REFLECTED ORDINARY WAVE
n_y
y
WAVE VECTOR FOR INCIDENT ORDINARY WAVE
n_x
E_z^{o}
E_y^{o}
E_x^{o}
n^{o}
x
PERFECTLY CONDUCTING PLANE Z = 0

Fig. 14

$$(\underset{\sim}{E}^{O} + c_{OO}\underset{\sim}{E}^{O'} + c_{OX}\underset{\sim}{E}^{X'}) \times \hat{z} = 0 \tag{23}$$

A similar constraint holds if the incident wave is purely extraordinary

$$(\underset{\sim}{E}^{X} + c_{XO}\underset{\sim}{E}^{O'} + c_{XX}\underset{\sim}{E}^{X'}) \times \hat{z} = 0 \tag{24}$$

The conversion of power between modes can be described by a matrix T of the form

$$[T] = \begin{bmatrix} |c_{OO}|^2 \frac{s_O'}{s_O} & |c_{OX}|^2 \frac{s_O'}{s_X} \\ |c_{XO}|^2 \frac{s_X'}{s_O} & |c_{XX}|^2 \frac{s_X'}{s_X} \end{bmatrix} \tag{25}$$

where s_O, s_X, s_O', s_X' are the power fluxes in the z direction for the ordinary and extraordinary mode incident and reflected wave eigenvectors,

$$\underset{\sim}{s} = \frac{1}{8\pi} \mathrm{Re}\{\underset{\sim}{E} \times (\underset{\sim}{n} \times \underset{\sim}{E}^{*})\} \tag{26}$$

The matrix T is symmetric by virtue of a reciprocity relation.

It was found that for plasma parameters characteristic of the surface plasma in EBT-I, a fraction approaching 1.0 of the energy in an incident wave can be mode-converted at certain angles. Figure 15 shows T_{OX} (fraction of incident ordinary mode energy converted to extraordinary mode) as a function of the polar angles of incidence $\phi = \tan^{-1}(n_y/n_x)$, $\theta = \tan^{-1}(n_z/\sqrt{n_x^2+n_y^2})$ for the case $\alpha = 0.05$, $\beta = 2.0$, $\psi = 90°$. These parameters would be appropriate near the mirror throat of EBT-I. Because the ordinary mode is so weakly damped in EBT-I, we may assume that the

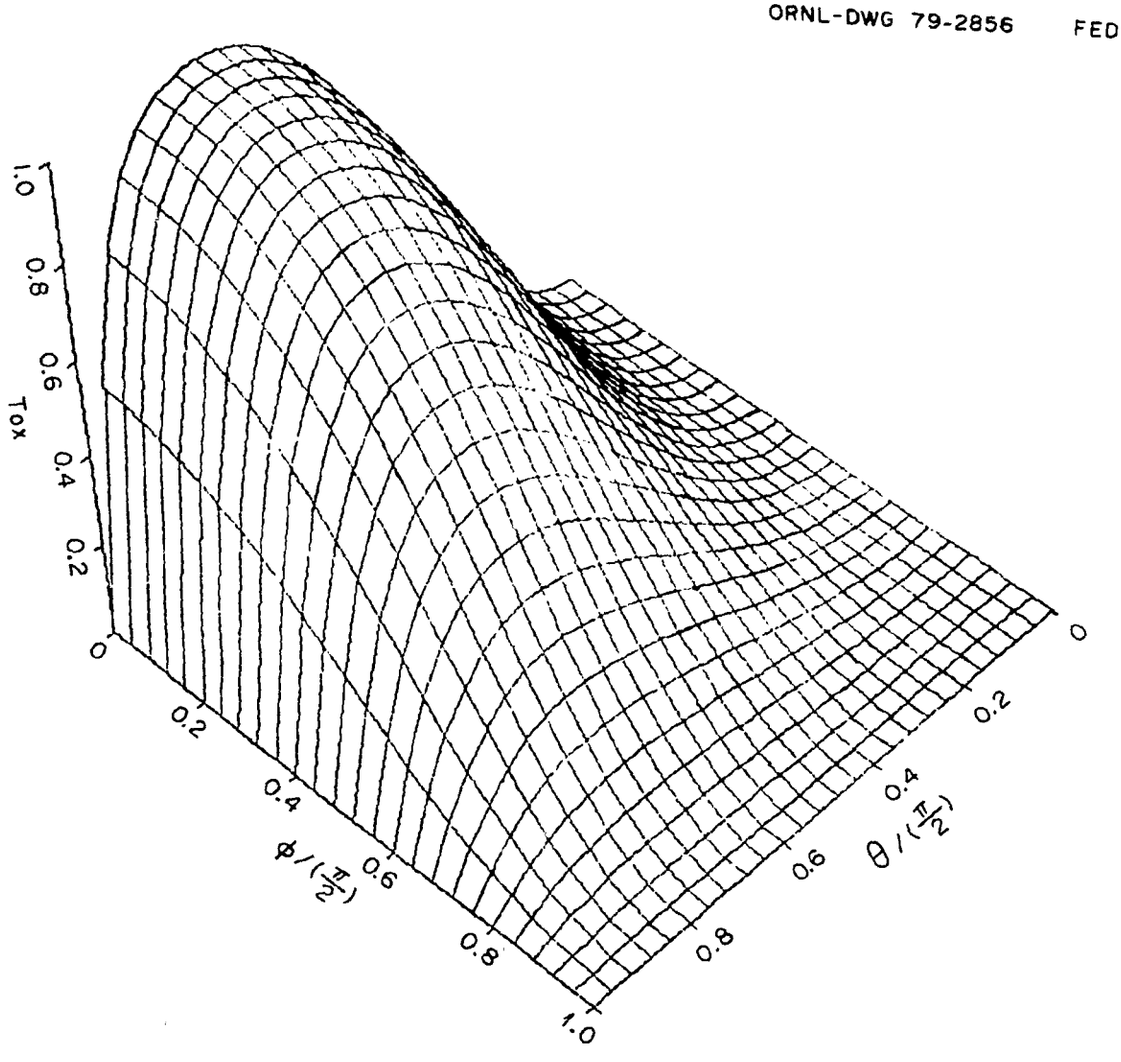
ORNL-DWG 79-2856 FED
Tox
1.0
0.8
0.6
0.4
0.2
0
0.2
0.4
0.6
0.8
1.0
$\phi/(\frac{\pi}{2})$
0
0.2
0.4
0.6
0.8
1.0
$\theta/(\frac{\pi}{2})$

Fig. 15

ordinary mode energy makes several wall bounces and the incident flux is nearly isotropic with respect to angle of arrival. If the mode conversion coefficient shown in Fig. 15 is averaged over a uniform, uncorrelated distribution of incident waves, one obtains $\langle T_{OX} \rangle = 0.403$ for the average fraction of ordinary mode power converted to extraordinary mode. Values of $\langle T_{OX} \rangle$ ranging from $\sim$0.1 to $\sim$0.5 are found throughout the α,β range to be expected in the high field part of the surface plasma. It should also be mentioned that this wall reflection process gives the minimum rate of mode conversion. Plasma inhomogeneities and turbulent fluctuations, particularly in the low density regions where $\underset{\sim}{n}^{O}$ and $\underset{\sim}{n}^{X}$ are nearly equal, will cause additional coupling between modes within the plasma. The extraordinary mode energy which is born in the high field region is rapidly absorbed upon propagating to the cyclotron resonance. Calculations of gross energy balance performed in [26] indicate that this process — propagation of ordinary mode to the high field region, conversion to extraordinary mode, and absorption of the extraordinary mode at the cyclotron resonance — is the dominant mechanism for heating of the core plasma in EBT-I. This view is supported by the experimental observation that the reflected power is lower and the plasma parameters are better when the dominant mode waveguides used to inject the microwaves are oriented so that the wave electric field is parallel to the magnetic field (ordinary mode) rather than perpendicular to it (extraordinary mode).

The results presented in the previous sections also have important implications for future EBT devices such as EBT-II. In hotter, denser devices the ordinary mode can do significant heating (Fig. 7b and Fig. 13).

This is advantageous because the dense plasma center is preferentially heated by the ordinary mode in contrast to the extraordinary mode which, when propagating from the high field side, is efficiently absorbed even in the cold, surface plasma. It is clear from Fig. 9c,d and 12 that the extraordinary mode will be heavily absorbed by the toroidal core plasma at the second harmonic resonance. The associated heating at the plasma edge may have deleterious effects on energy transport and impurity behavior. In addition, the effects which the presence of a hot, dissipative plasma at the second harmonic resonance will have on the formation and maintenance of the annulus are not at all understood.

ACKNOWLEDGMENTS

The authors would like to express appreciation for the valuable ideas and information gained in discussions with R. A. Dandl, N. H. Lazar, H. O. Eason, C. L. Hedrick, H. Weitzner, and A. H. Kritz.

REFERENCES

[1] DANDL, R.A., EASON, H.O., GUEST, G.E., HEDRICK, C.L., IKEGAMI, H., NELSON, D.B., in Plasma Physics and Controlled Nuclear Fusion Research (Proc. 5th Int. Conf. Tokyo, 1974), Vol. 2, IAEA, Vienna (1975) 141; DANDL, R.A., DORY, R.A., EASON, H.O., GUEST, G.E., Research Program for Plasma Confinement and Heating in ELMO Bumpy Torus Devices, Oak Ridge National Laboratory Rep. ORNL/TM-4941 (June 1975).

[2] DANDL, R.A., EASON, H.O., IKEGAMI, H., Electron-Cyclotron Heating of Toroidal Plasma with Emphasis on Results from the ELMO Bumpy Torus (EBT), Oak Ridge National Laboratory Rep. ORNL/TM-6703 (May 1979).

[3] BAITY, F.W., BECKER, M.C., CARPENTER, K.H., COBBLE, J.A., EASON, H.O., et al., Summary of EBT-I Experimental Results, Oak Ridge National Laboratory Rep. ORNL/TM-6457 (October 1978).

[4] JAEGER, E.F., SPONG, D.A., HEDRICK, C.L., Phys. Rev. Lett. 40 (1978) 866.

[5] McALEES, D.G., UCKAN, N.A., BETTIS, E.S., HEDRICK, C.L., JAEGER, E.F., et al., The ELMO Bumpy Torus Reactor (EBTR) Reference Design, Oak Ridge National Laboratory Rep. ORNL/TM-5669 (November 1976).

[6] GRAWE, H., Plasma Phys. 11 (1969) 151.

[7] ELDRIDGE, O.C., Phys. Fluids 15 (1972) 676.

[8] BRAMBILLA, M., Plasma Phys. 10 (1968) 359.

[9] SPROTT, J.C., Phys. Fluids 14 (1971) 1795.

[10] KUKES, A.F., Plasma Phys. 10 (1968) 367.

[11] ALIKAEV, V.V., Perspectives on Utilization of Electron-Cyclotron Waves for Heating Plasmas in Large-scale Devices of the Type 'Tokamak,' IAE-2610, Moscow (1976).

[12] LITVAK, A.G., PERMITIN, G.V., SUVOROV, E.V., FRAJMAN, A.A., et al., Nucl. Fusion 17 (1977) 659.

[13] ELDRIDGE, O.C., NAMKUNG, W., ENGLAND, A.C., Electron Cyclotron Heating in Tokamaks, Oak Ridge National Laboratory Rep. ORNL/TM-6052 (November 1977); to be published in Phys. Fluids.

[14] FIDONE, I., GRANATA, G., MEYER, R.L., Phys. Fluids 21 (1978) 645.

[15] ANTONSEN, Jr., T.M., MANHEIMER, W.M., Phys. Fluids 21 (1978) 2295.

[16] BORNATICI, M., ENGELMANN, F., Radio Sci. 14 (1979) 309.

[17] BATCHELOR, D.B., GOLDFINGER, R.C., Rays: A Geometrical Optics Code for EBT, Oak Ridge National Laboratory Rep. ORNL/TM-6844 (1979; in press).

[18] STIX, T.H., The Theory of Plasma Waves, McGraw-Hill, New York (1962).

[19] AKHIEZER, A.I., AKHIEZER, I.A., POLOVIN, R.V., SITENKO, A.G., STEPANOV, K.N., et al., Plasma Electrodynamics, Vol. I, Pergamon Press, Oxford (1975).

[20] SHKAROFSKY, I.P., Phys. Fluids 9 (1966) 561.

[21] BERNSTEIN, I.B., Phys. Fluids 18 (1975) 320.

[22] Olson has investigated the multiple roots in this region for the case $\theta = 0$. OLSON, C.L., Ph.D. dissertation, University of California, Los Angeles (1970).

[23] BAITY, F.W., BALLOU, J.K., BATCHELOR, D.B., BETTIS, E.S., CAMPBELL, D.B., et al., The EBT-II Conceptual Design Study, Oak Ridge National Laboratory Rep. ORNL/TM-5955 (1978).

[24] BUDDEN, K.G., Radio Waves in the Ionosphere, Cambridge University Press, Cambridge (1961).

[25] BATCHELOR, D.B., Budden Tunnelling in Parallel Stratified Plasmas, Oak Ridge National Laboratory Rep. ORNL/TM-6796 (1979); submitted to Plasma Phys.

[26] BATCHELOR, D.B., A Simple Power Balance Model for Microwave Heating in EBT, Oak Ridge National Laboratory Rep. ORNL/TM-7001 (in preparation).

LIST OF FIGURES

FIG. 9. Fraction of power absorbed from a ray passing through second harmonic resonance for plasma parameters characteristic of EBT-II.

FIG. 10. Extraordinary mode propagation in EBT-I. Numbers by rays indicate fraction of power absorbed.

FIG. 11. Ordinary mode propagation in EBT-I. Numbers by rays indicate fraction of power absorbed.

FIG. 12. Extraordinary mode propagation in EBT-II. Cross marks indicate 10%, 20%, ... absorption.

FIG. 13. Ordinary mode propagation in EBT-II. Cross marks indicate 10%, 20%, ... absorption.

FIG. 14. Geometry for wave depolarization upon wall reflection.

FIG. 15. Power conversion coefficient T_{OX} from ordinary to extraordinary mode vs angle of incidence. The plasma parameters are characteristic of the mirror throat region of EBT-I. $\langle T_{OX} \rangle = 0.403$.